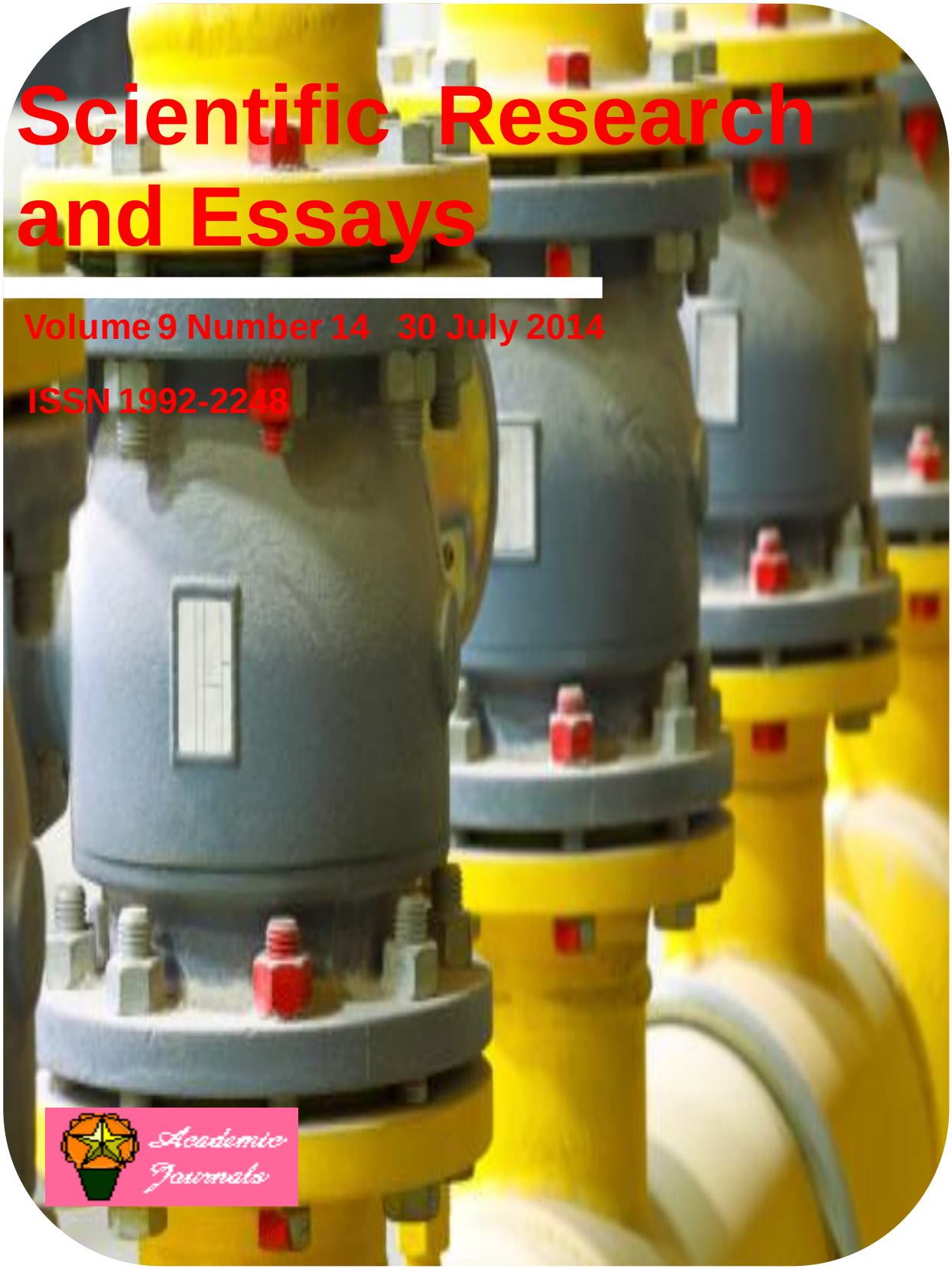

Scientific Research and Essays

Volume 9 Number 14 30 July 2014

ISSN 1992-2248

Academic Journals

ABOUT SRE

The **Scientific Research and Essays (SRE)** is published twice monthly (one volume per year) by Academic Journals.

Scientific Research and Essays (SRE) is an open access journal with the objective of publishing quality research articles in science, medicine, agriculture and engineering such as Nanotechnology, Climate Change and Global Warming, Air Pollution Management and Electronics etc. All papers published by SRE are blind peer reviewed.

Submission of Manuscript

Submit manuscripts as e-mail attachment to the Editorial Office at: sre@academicjournals.org. A manuscript number will be mailed to the corresponding author shortly after submission.

The Scientific Research and Essays will only accept manuscripts submitted as e-mail attachments.

Please read the **Instructions for Authors** before submitting your manuscript. The manuscript files should be given the last name of the first author.

Editors

Editorial Board

n detail.

Fees and Charges: Authors are required to pay a $550 handling fee. Publication of an article in the Scientific Research and Essays is not contingent upon the author's ability to pay the charges. Neither is acceptance to pay the handling fee a guarantee that the paper will be accepted for publication. Authors may still request (in advance) that the editorial office waive some of the handling fee under special circumstances.

Submission of a manuscript implies: that the work described has not been published before (except in the form of an abstract or as part of a published lecture, or thesis) that it is not under consideration for publication elsewhere; that if and when the manuscript is accepted for publication, the authors agree to automatic transfer of the copyright to the publisher.

Scientific Research and Essays

Table of Contents: Volume 9 Number 14 30 July, 2014

ARTICLES

Research Articles

academicJournals

Vol. 9(14), pp. 628-633, 30 July, 2014
DOI: 10.5897/SRE2014.6046
Article Number: 5B986D446443
ISSN 1992-2248 © 2014

http://www.academicjournals.org/SRE

Scientific Research and Essays

Full Length Research Paper

Evaluation of antiemetic effect of aqueous rhizome extract of *Cynodon dactylon* against all emetogenic stimuli

Imran Ahmad Khan[1]*, Abdul Aziz[1], Muzammal Sattar[2], Shaukat Hussain Munawar[3], Zahid Manzoor[3], Muhammad Asif Raza[4] and Ghayoor Fatima[5]

[1]Faculty of Pharmacy, Bahauddin Zakariya University, Multan, Pakistan.
[2]Departmnent of Physiology and Pharmacology, University of Agriculture, Faisal Abad, Pakistan.
[3]Faculty of Medicine and Allied Medical Sciences, Isra University, Islamabad, Pakistan.
[4]The Ghazi University, Dera Ghazi Khan, Pakistan.
[5]Organic Plant Production and Agroecosystems Research in the Tropics and Subtropics, University of Kassel, Germany.

Received 30 April, 2014; Accepted 2 July, 2014

This study was an extension of our previous antiemetic work. Many researchers quoted *Cynodone dactylon* as anti emetic agent but none of them have provided strong pharmacological evidence for it, which drove us for its therapeutic evaluation. Crude aqueous rhizome extract of *C. dactylon* was evaluated for anti-emetic activity. Emesis was induced by the oral administration of copper sulphate, fresh aqueous extract of *Brasica compestris* while intravenous Cisplatin was used to induce emesis in fifteen days age chicks of either sex. The anti-emetic activity was determined by calculating the mean decrease in number of emesis in comparison to those of control and standards. *C. dactylon* (50 and 100 mg/kg body weight orally) showed remarkable emesis suppressant activity when compared with standard drugs chlorpromazine, domperidone and metoclopramide. Both the doses showed remarkable antiemetic activity.

Key words: Antiemetic, *Cynodone dactylon,* chick emesis model, domperidone, metoclopramide, chlorpromazine, *Brasica compestris*.

INTRODUCTION

Vomiting is a means by which gastrointestinal tract rids itself of its contents when upper gastro intestinal tract (GIT) excessively irritated, over distend or even over excited (Guyton and Hall, 2011). Irritation on the small area located bilaterally on the floor of the fourth ventricle in or above the area postrema causes vomiting which is

*Corresponding author. E-mail: imranahmadkhadurrani@gmail.com. Tel: 923336120602.

located in medulla (Shahzad, 2011). Chemorecepter trigger zone gets excited with artificial electrical stimulation and drugs (Morphine, digitalis derivatives and chemotherapeutic agents). Motion sickness and classical migraine quite often excite chemorecepter trigger zone for vomiting (Kumar and Clark, 2002). Cholera toxin, irritable bowel syndrome and gestro-eosophygeal reflux disease (www.bnf.org), partial or complete bowel obstruction, uremia and brain metastases are also contributing factors (www.pakcancer.com). Electrolyte imbalance such as hyponatrremia, hypercalicemia and hyperglycemia induces emesis (www.cancer.org). Muscarinic M_1, histaminic H_1, neurokinin NK_1 and serotonin $5HT_3$ receptors nucleus tractus solitaries are involved while in area postrema dopamine D2, Opioid, serotonin $5HT_3$ neurokinin NK_1 receptors are responsible for ematogenic response (Katzung, 2011).

Cynodon dactylon belongs to the family of Poaceae (Saroja and Annapoorani, 2012). It is said to have many medicinal properties including antihelmentic (Sujon et al., 2008), antidiuretic, antinflammatory and hepatoprotective activity (Singh et al., 2009), efficacious for prostatitis and dysentery (Cheryl, 206). Traditionally, it is used in diabetes (Jarald et al., 2008; Singh et al., 2007), jaundice, kidney problems (Khajavi et al., 2011), urinary disease, constipation and abdominal pain (Das and Dutta, 2011). The whole plant is used for diuretic, dropsy, syphilis, wound infection and piles, anti haemorrhagic, in dysentery and nasal bleeding (Kunja et al., 2012). The juice of the plant is astringent and is applied externally to fresh cuts and wounds. It is used in the treatment of catarrhal opthalmia, hysteria, epilepsy, insanity, and chronic diarrhea (Rad et al., 2011). The plant is folk remedy for anasarca, calculus, carbuncles, cough, hypertension, snake bites, gout and rheumatic affections (Najafi et al., 2008). *C. dactylon* is a valuable herbal medicine and used for first aid for minor injuries (Oudhia et al., 1998). *C. dactylon* is bitter, sharp hot taste, good odour, laxative, brain and heart tonic, aphrodisiac, expectorant, carminative and useful against grippe in children and for pains, inflammations and toothache (Oudhia, 1999a). In homoeopathic systems of medicine, it is used to treat all types of bleeding and skin troubles (Agharkar, 1999). It is reported to have anticonvulsant effect (Oudhia, 1999b). It is also known for its antidiabetic and hypolipidemic effect (Santosh et al., 2007). Its antimicrobial and antifungal potentials were also reported (Kanimozhi and Ratha, 2012). It is also reported as anti inflammatory agent (Garg and Khosa, 2008). New antiemetic agents are the need of the time which effectively counters multiple emetogenic stimuli. *C. dectylone* is known as good antiemetic agent locally but yet do not have strong pharmacological evidence for this, which was the main aim of this evaluation. In this study, the antiemetic activity of aqueous rhizome extract of *C. dactylon* was tested against multiple emetogens.

MATERIALS AND METHODS

Collection of plant material

Indigenous medicinal plant *C. dactylon* is known by its local name of “Dub grass”. The plant was collected from the fields of Multan, Pakistan. The plant material was authenticated by Professor of Pharmacognosy, Dr. Romana Riaz at Multan college of Pharmacy, Multan, Pakistan.

Crude extract

The subterranean parts of *C. dactylon* were washed with fresh water, dried under shade at room temperature and grinded to form coarse powder. The powdered sample (100 g/100 ml) were kept in aqueous solvent (water) overnight at room temperature, filtered through muslin cloth then through Wattman-1 filter paper. The extract was evaporated at 50°C until a paste like consistency was attained (Khan et al., 2014).

Chemicals

They include: Copper (Scharlau Chem-ie S.A. Barcelona, Spain), dimethyl sulfoxide (DMSO) and polyoxy-ethylene sorbitan monooleate (Tween 80) (Darm-stadt, Germany), chlorpromazine and Metoclopramide (GSK Pharmaceutical (pvt). Ltd, Pakistan), Domperidone (Johson & Johnson Pharmaceuticals (Pvt) Ltd. Karachi, Pakistan), cisplatin (Sanofi aventis Pharmaceuticals (pvt) Ltd. Pakistan).

Animals

Chicks of either sex, fifteen days of age, weighing from 332 to 345 g were obtained from Al -Manara poultry traders, Multan. After 12 h fasting (deprived of food but had free access to water), the antiemetic activity was conducted. All chicks were kept under laboratory conditions at room temperature with 12 h light and dark cycles. All animal experiments were carried out in accordance with the acts of the Animal Ethical Committee of Multan College of Pharmacy, Multan, Pakistan (EC. rab /11/2013)

Antiemetic activity

Brasica compestris induced emesis model

Same procedure was adopted for fresh aqueous extract of *Brasica compestris* induced emesis as described by Imran et al. (2014). Chicks were divided into 6 groups, 3 chicks in each group. Each chick was placed in a large separate beaker and left to settle for 10 min. Aqueous extracts of *C. dactylone*. were prepared to a dose of 50 and 100 mg/kg body weight in a volume of 10 ml/kg in 0.9% saline containing 5% DMSO and 1% Tween 80. The doses were administered orally. The control group received vehicle (0.9% containing 5% DMSO and 1% Tween 80). After 10 min, fresh leaves extract of *B. compestris* was administered orally to irritate gastric mucosa. The number of retches was observed during the next 10 min. Chlorpromazine, domperidone and metoclopramide were used as standard antiemetic drugs (150, 100, 50 mg/kg body weight, respectively).

Cisplatin induced emesis model

Cisplatin induced model was used in fifteen days old chicks of

either sex according to Florczyk et al. (1982). Cisplatin 10 mg/kg was given by IV catherter. Other protocol remained same as before.

Copper sulphate induced emesis model

The antiemetic activity was evaluated by using chick emesis model (Khan et al., 2013). Copper sulphate at a dose of 50 mg/kg b.w was used to stimulate peripheral nervous system for emesis. Other protocol remained same before. The percent inhibition was calculated by the following formula:

Inhibition (%) = (A – B / A) × 100

Where A = Frequency of retching in control group and B = Frequency of retching in test group.

Phytochemical study

Phytochemical analysis for the presence of various phytochemical classes was done by the method described by Aziz et al. (2013).

Toxicity study

C. dactylon was evaluated for the toxic effects and toxic dose in albino rats. Albino rats were divided in 4 (a, b, c, d) groups, with each group containing 5 rats. Group 'a' was treated with distilled water while other three were given 1100, 2200, 3300 mg/kg body weight of *C. dactylon*. Physiological, biochemical and haematological parameters were analysed as per standard procedures. *C. dactylon* was found to be safe dose up to 3300 mg/kg body weight in albino rats.

Statistical analysis

Values for antiemetic activity was expressed as mean ± standard error of mean (SEM). The statistical significance was determined by an unpaired Student's *t*-test where *P* values of < 0.05 were considered significant and < 0.01 were highly significant.

RESULTS

Preliminary phytochemical screening detected presence of tannins, phenols, saponins, anthraquinones and coumarins as constituents of the crude aqueous rhizome extract of *C. dactylon* as depicted in Table 1. Results of the antiemetic activity of aqueous extracts of *C. dactylon* at both concentrations are given in Figures 1 to 3. Both the extracts inhibited emesis to an extent greater than chlorpromazine at a dose of 150 mg/kg. At test dose of 50 mg/kg, *C. dactylon* showed more antiemetic activity as compared to the reference drug, chlorpromazine, against brasica and copper sulphate induced models and slightly less in cisplatin induced model as given in Figures 1 to 3, while metoclopramide and domperidone showed more potential in suppression against all induced models in comparison to respective dose 50 mg/kg. At test dose of 100 mg/kg, *C. dactylon* showed almost similar antiemetic activity as metoclopramide and domperidone reference drugs as shown in Figures 1 to 3, respectively. In copper sulphate induced model, highest antiemetic activity showed by *C. dactylon* was 79.41% and the lowest was 52.94%. In fresh *Brasica* aqueous extract induced model, highest antiemetic was observed (81.91%) and lowest (59.57%). In cisplatin induced model, highest antiemetic response was (75.38%) and lowest (60.03%) was observed.

DISCUSSION

Diversified multiple receptors blocking mechanism was most likely to be the cause of such effective suppression of ematogenic stimuli. *C. dactylon* blocked $5HT_3$ receptors of small intestine so entereochromaffin cells failed to release serotonin which is responsible for vagal stimulation which in turn initiates vomiting reflex. Its bronchspasm revealing activity supports this claim (Patel et al., 2013). *C. dactylon* blocked the H_1 receptors of gastric mucosa so that thiocynates of *Brasica* failed to stimulate H_1 receptors and release of histamine by irritation which would in turn stimulate chemotrigger zone of medulla for emesis. Anti allergy activity of *C. dactylon* supports this claim (Subramanian et al., 1986; Anonymous, 1978). Radiation induces emesis by irritating gastric mucosa especially small intestine which is similar to cynates of Brasica, which provides its effectiveness in post radiation induced emesis.

Acetylcholine is one of the neurotransmitter involved in emesis (www.cnnj.org), while *dactylone* antidirrheal activity have already been reported via anticholinergic mechanism which is an effective evidence for antiemetogenic response of it (Oudhia et al., 1998) as anticholinergics are good choice of antemetic medications (Michelle et al., 2011). Although the results are significant but the mode of action is not exactly known. However, proposed mechanisms are as the oral copper sulphate which induces emesis by peripheral action (Hossein et al., 2005) and the extracts were able to effectively prevent its effect, it could be implied that these extracts have a peripheral anti-emetic action. Brasica induces emesis by the toxic effect of its phytoconstituent isothiocynate and betaphenylisothiocynate (Decker, 1971; Mishra et al., 2012) by causing irritation in the gastrointestinal mucosa. This irritation causes release of histamine and serotonin as vomiting centre rich in H_1-histamine receptors (Katzung, 2011), while in other way input to the vomiting centre are generated by vagus and spinal nerves of the gastric mucosa which are rich in $5HT_3$ receptors. This potentiates ematogenic stimuli in the brain by stimulating vagus afferent input to the vomiting centre.

Cisplatin and other chemotherapeutic agents induces emesis by stimulating the 5HT M-receptors located on

Table 1. Pytochemical analysis of aqueous rhizome extract of *C. dactylon*.

S/No	Test	Observations	Result
1	Alkaloid	orange ppt	Positive
2	Steroids	Violet colour	Positive
3	Tannins	Dark green colour	Positive
4	Glycoside	Pink	Positive
5	Saponin	1 cm froth	Positive
6	Phenols	Light purple	Positive
7	Flavanoid	yellow	Positive

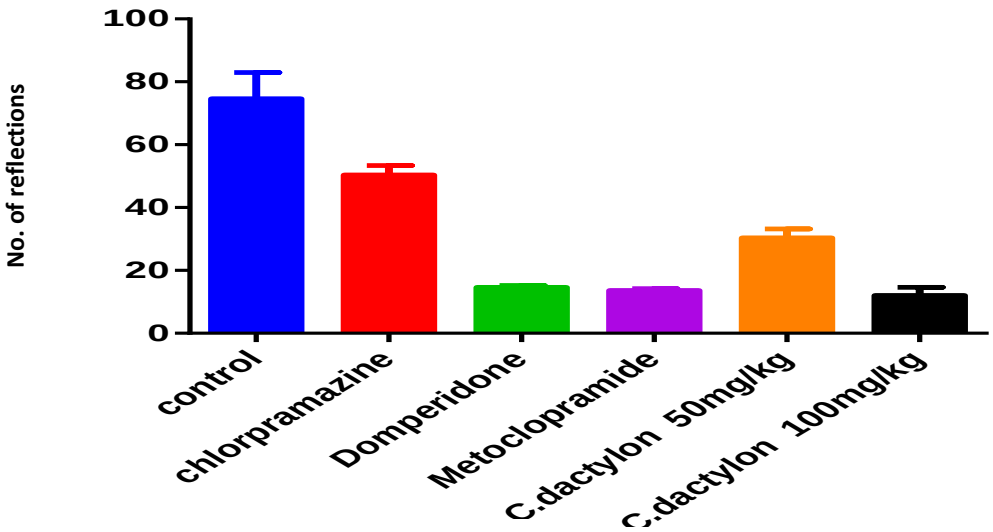

Figure 1. Effect of drugs on copper sulphate emesis. Antiemetic effect, Group-I: Control (Distilled Water); Group-II: Standard drugs (Chlorpromazine, metoclopramide and domperidone); Group-III; *C. dactylon* (50 and 100 mg/kg).

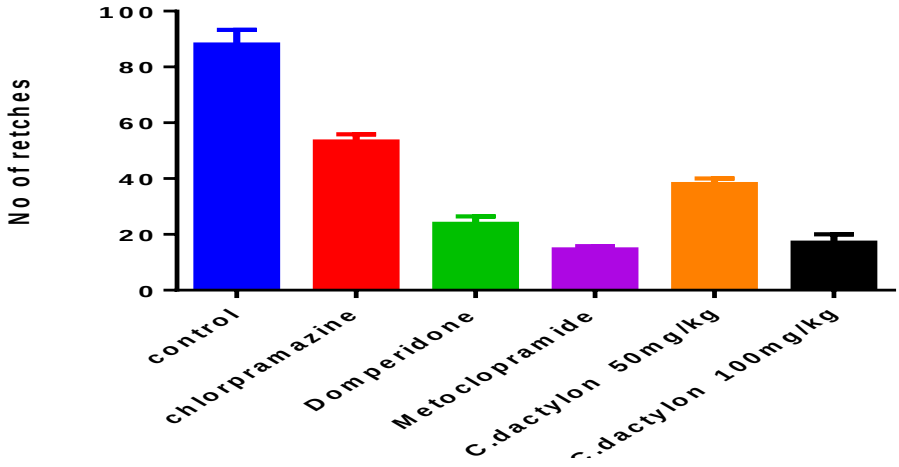

Figure 2. Effects of drugs on Brasica compestris induced emesis. Antiemetic effect, Group-I: Control (distilled water); Group-II: Standard drugs (chlorpromazine, metoclopramide and domperidone); Group-III; *C. dactylon* (50 and 100 mg/kg).

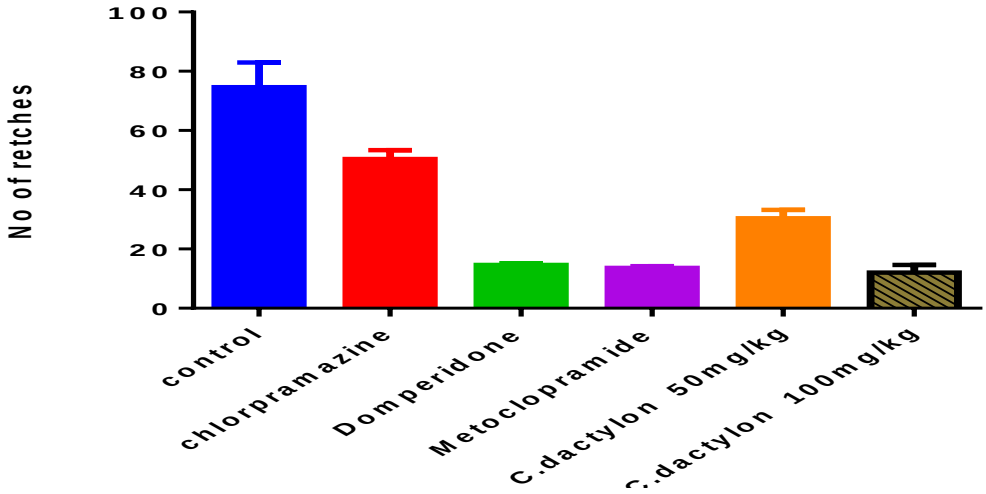

Figure 3. Antiemetic effect, Group-I: Control (distilled water); Group-II: Standard drugs (chlorpromazine, metoclopramide and domperidone); Group-III; *C. dactylon* (50 and 100 mg/kg).

afferent nerve pathways leading from the viscera to the area postrema. Our study verified the results that domperidone are most strongly dopamine receptor mediated in activity but metoclopramide in high dose blocks the 5HT-M receptors which was the cause of chemotherapy induced emesis (Wesley et al., 1986). *Cynodon dactylon* is rich in plant steroids (Abdullah et al., 2012) and steroids are used in combination to prevent emetic stimuli (Katzung, 2012; BNF, 2012) which helps in countering the emetic effect of cisplatin along 5HT-M receptor blockade.

CONCLUSION

From the present investigation it is clear that *C. dactylon* aqueous rhizome extract possess excellent antiemetic activity. Others factors such as the sex, emetogenic stimulation site and type of stimuli did not affect the degree of antiemetic activity due to its multidisciplinary receptor blocking mechanism.

Conflict of interest

The authors have not declared any conflict of interests.

REFERENCES

Abdullah S, Gobilik J, Chong KP (2012). Preliminary Phytochemical Study and Antimicrobial Activity from Various Extract of Cynodon Dactylon (L.) Pers. (Bermuda) Against Selected Pathogens. Int. J. Pharm. Pharm. Sci. 4(5):227-230.

Agharkar SP (1999). Medicinal plants of Bombay presidency. Sci. Publ. Jodhpur, India. pp. 80-87. Anonymous (1978). The Ayurvedic Formulary of India, Ministry of Health and Family Planning, Govt. of India, New Delhi, Part-1:249.

Aziz A, Khan IA, Munawar SH, Munzoor Z, Agha S (2013). Evaluation of antitussive activity of Lycopus europaeus on cough reflex induced by different cough induced models in mice. Int. J. Pharm. Sci. 3(6):412-416.

Cheryl AL (2006). Ethnomedicines used in Trinidad and Tobago for urinary problems and Diabetes mellitus. J. Ethnobiol. Ethnomed. 45(2):1746-4269.

Das S, Dutta CM (2010). Plants Used Against Gastro-Intestinal Disorders and As Anti Hemorrhagic by Three Tribes of North Tripura District, Tripura, India. Ethnobot. Leaflets 10(4):467-478.

Decker WJ (1971). In Quest of Emesis: Fact, Fable and Fancy. Clin. Toxicol. 4(3):383–387. http://dx.doi.org/10.3109/15563657108990490

Garg VK, Khosa RL (2008). Studied the Analgesic and Anti-Pyretic activity of aqueous extract of Cynodon dactylon. Pharmacologyonline 3(1):12-18.

Florczyk AP, Schurig JE, Bradner WT (1982). Cisplatin-induced emesis in the ferret. A new animal model. Cancer Treat. Rep. 66(3):187-189.

Guyton C, Hall JE (2011). Textbook of medical physiology (11th ed.) ELSVIER, Philadelphia . p. 823.

Hossein H, Mashallah M, Akbar G (2005). Antiemetic effect of Mentha xpiperita aerial parts extracts in young chickens. Iran. J. Pharm. Sci. 15(1):21-24.

Imran AK, Aziz A, Sarwar HS, Munawar SH, Manzoor Z, Anwar H (2014). Evaluation of antiemetic potential of aqueous bark extract of Cinnamon loureiroi. Can. J. App. Sci. 4(1):26-32.

Jarald EE, Joshi SB, Jain, DC (2008). Antidiabetic activity of aqueous extract and non polysaccharide fraction on Cynodon dactylon Pers. Indian J. Exp. Biol. 46(9):660-667.

Khajavi RA, Hadzadeh MA, Rajaei Z, Mohammadian N, Valiollahi S, Sonei M (2011). The beneficial effect of Cynodon dactylon on ethylene glycol-induced kidney calculi in rats. Urol. J. 8(3):179-184.

Kanimozhi D, Ratha BV (2012). Evaluation of Anti Microbial Activity of Cynodon dactylon. IJRPS 2(2):34-43.

Katzung GB (2011). Basic and clinical Pharmacology (11th edi.) Lange Medical Publications, USA. 1084.

Khan IA, Aziz A, Munawar SH, Munzoor Z (2013). Antiemetic Activity of Methanolic Leaf Extract of Rumex Vesicarius Linn. Int. J. Pharm. Res. All. Sci. 2(4):33-37.

Khan IA, Aziz A, Munawar SM, Manzoor Z, Sarwar HS, Afzal A, Raza MA (2014). Study on antipyretic activity of Rumex vesicarius leaves extract in albino rabbits. Vet. World 3(1):44-48.

http://dx.doi.org/10.14202/vetworld.2014.44-48
Kumar P, Clark M (2002). Clinical Medicine (6th edi) W.B Saunders, England. p. 253.
Kunja B, Satapathy BB, Sahu GS (2012). Crop weeds diversity and their ethnomedicinal uses in the treatment of common ailments in Jaipur district of Odisha (India). Int. J. Med. Arom. Plants 2(1):80-89.
Mishra A, Dash P, Murthy PN, Siddique HH, Kushwaha P (2012). A Classical Review on Rajika (Brassica juncea Research and Reviews. J. Bot. Sci. 6(2):45-49.
Michelle A, Clark C, Richard A, Harvey S, Richard F, Jose A, Karen W (2011). Lippincott illustrated review clinical pharmacology: Lippincott Williams & Wilkins (5th)
Najafi M, Nazemiyeh H, Ghavimi H, Gharakhani A, Garjani A (2008) Effects of hydroalcoholic extract of Cynodon dactylon (L.) pers. On ischemia/reperfusion-induced arrhythmias. DARU 16(4):233-237.
Oudhia P (1999). Medicinal weeds in rice fields of Chhattisgarh (India). Int. Rice Res. 24(1):40.
Oudhia P (1999). Medicinal weeds in groundnut fields of Chhattisgarh (India). Int. Arachis Newslett. 19(1):62-64.
Oudhia P, Joshi BS, Kosta VK (1998). The possibilities of preparing homeopathic drugs from the obnoxious weeds of Chhattisgarh. Bhartiya Krishi Anusandhan Patrika 13(1/2):53-57.
Patel MR, Bhalodia YS, Pathak NL, Patel MS, Suthar K, Patel N, Golwala DK, Jivani NP (2013). Study on the mechanism of the bronchodilatory effects of Cynodon dactylon (Linn.) and identification of the active ingredient. J. Ethnopharmacol. 150(3):946-952. http://dx.doi.org/10.1016/j.jep.2013.09.053
Rad AK, Hadjzadeh MA, Rajaei Z, Mohammadian N, Valiollahi S, Sonei M (2011) The Beneficial Effect of Cynodon Dactylon Fractions on Ethylene Glycol-Induced Kidney Calculi in Rats. Urol. J. 8:179-184.
Shahzad GR (2011). Concise Physiology (1st edi) Friends Publishers, Pakistan. p. 375.
Saroja M, Annapoorani SA (2012). Antitumor activity of methanolic extract of Cynodon dactylon leaves against ehrlich ascites induced carcinoma in mice. J. Adv. Sci. Res. 3(1):105-108.
Sujon MA, Mostofa M, Jahan MS, Das AR, Rob S (2008). Studies on Medicinal plants against Gastrointestinal Nematodes of Goats. Bangl. J. Vet. Med. 6(2):179-183.
Singh SK, Rai PK, Mehta S, Singh RK, Watal G (2009). Curative effect of Cynodon dactylon against Stz induced hepatic injury in diabetic rats. Indian J. Clin. Biochem. 24(4):410-413.http://dx.doi.org/10.1007/s12291-009-0073-3
Singh SK, Kesari AN, Gupta RK, Jaiswal D, Watal G (2007). Assessment of antidiabetic potential of Cynodon dactylon extract in streptozotocin diabetic rats. J. Ethnopharmacol. 114(2):174-179.
http://dx.doi.org/10.1016/j.jep.2007.07.039
Santosh KS, Prashant KR, Dolly J, Geeta W (2007). Evidence based Critical Evaluation of Glycemic Potential of Cynodon dactylon. Evid. Based Complem. Altern. Med. 5(4):415-420.
Subramanian S, Nagarajan S, Sarathi M, Rajesh KS (1986). Studied the Wound healing properties of Cynodon dactylon and Pongamia glabra (18th Annual Conference of Indian Pharmacol. Soc. Indian J. Pharmacol. 18 (1):19-60.
Wesley D, Miner F, Gareth J, Sanger S (1986). Inhibition of cisplatin-induced vomiting by selective 5-hydroxytryptamine M-receptor antagonism. Br. J. Pharmacol. 88(3):497-499.http://dx.doi.org/10.1111/j.1476-5381.1986.tb10228.x
www.bnf.org/coping/types/page . Accessed 26 December 2013
www.Pakcancer.com/coping/types/page. Accessed 26 December 2013
www.cancer.gov/cancertopics/coping/eatinghints/page. Accessed 26 December 2013

academicJournals

Vol. 9(14), pp. 634-644, 30 July, 2014
DOI: 10.5897/SRE2014.5942
Article Number: 3F4F39946445
ISSN 1992-2248 © 2014

http://www.academicjournals.org/SRE

Scientific Research and Essays

Full Length Research Paper

Bearing characteristics and influencing factors analysis of bored pile under refreezing condition in permafrost region

Zhang Junwei[1,2]*, Zeng Yi[1], Ma Xiaojie[3] and Li Lei[1]

[1]School of Geoscience and Technology, Southwest Petroleum University, Chengdu, 610500, China.
[2]State Key Laboratory for GeoMechanics and Deep Underground Engineering, China University of Mining and Technology, Beijing, China
[3]Zhejiang College of Construction, Hangzhou, 311231, China.

Received 22 April, 2014; Accepted 15 July, 2014

This paper represents study results of the bearing characteristics and influencing factors of large diameter bored pile under refreezing condition in permafrost region. Principles for designing piles in permafrost on the basis of both ultimate capacity and limiting deformations are first reviewed. To solve problems such as pile cap and bridge pier construction, super structure construction, time limit construction, a field experiment was carried out on both the bearing capacity and deformation characteristic of large diameter bored pile in high-temperature fine-granular frozen soil of Fenghuoshan region of the Qinghai-Tibet plateau. Based on ground temperature and *in-situ* experiment data, pile tip resistance accounted for the entire load is just 2.5% when load on pile top reached 6000 kN after frozen soil refreezing was completed. In the meantime, it was also observed that the deformation features of refreezing large diameter bored pile in permafrost. The bored pile is a typical friction pile of the friction pile characterized by the settlement characteristic that pile tip resistance had less loading sharing ratio. The results also indicated that it was very difficult for the permafrost to refreeze to the original state as soon as it had been disturbed due to the bored pile construction. Also, pile shaft force and pile side resistance were connected to pile top loading, characteristic of frozen soil around the pile and ground temperature. The study results can be used as some guides and references in the process of pile foundation construction.

Key words: bored pile, permafrost, pile side resistance, pile bearing capacity

INTRODUCTION

Qinghai-Tibet railway with a length of 1118 km has been completed across the permafrost hinterland of the Qinghai-Tibet Plateau between Golmud and Lhasa in 2008. Some 630 km of the railway run across permafrost with a mean annual air temperature of -7 to -2°C. Permafrost, as a term used to describe permanently frozen ground, indicates a thermal condition where the temperature of the rock or soil remains below freezing

*Corresponding author. Email: zhanggjunwei@gmail.com

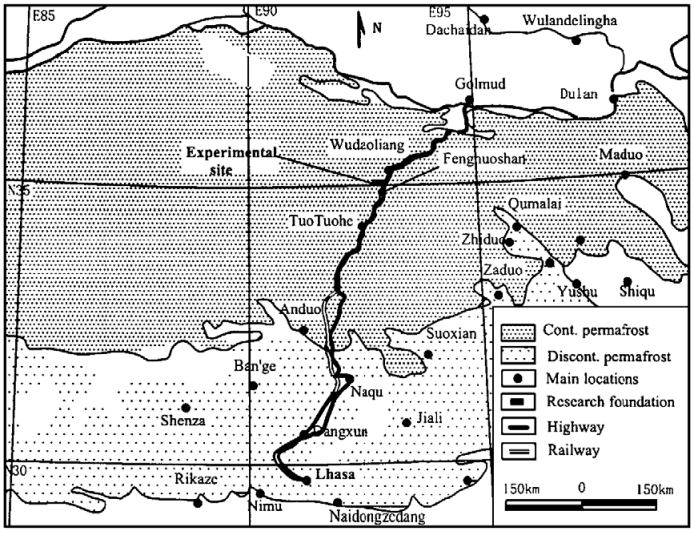

Figure 1. Test site of bored pile in the Qinghai-Tibet Plateau Permafrost.

throughout the year. Permafrost can exist for as few as three years to more than tens of thousands of years (Biggar and Kong, 2001; Suleiman et al., 2006; Zhang et al., 2008; JGJ118, 2011). About one-fifth of the earth's land mass contains permafrost. Almost one-half of the world's permanently frozen ground is in Alaska, Russia and Siberia, one-third is in Canada, and a large portion is in Qinghai-Tibet plateau and Northeast of China. Disturbing permafrost carelessly may cause thaw, resulting in uneven foundation settling and disastrous consequences for the building. And it is not always possible to safely build on permafrost. Permafrost can either be continuous or permanent. Changes in climate and construction disturbance may cause permafrost to thaw and disappear (Wang et al., 2013; Xiuli et al., 2012; Yao et al., 2012; Wang et al., 2008). Consequently, the ramifications for foundation design and particularly pile foundation design in permafrost are very significant, otherwise may bring about a great reduction in allowable load for foundations in permafrost (Zhu et al., 1982; Niu and Liu, 2004). Foundation design in permafrost must reckon with both thermal and rheological considerations.

However, bored pile, as an important foundation type in permafrost regions, can increase stability of bridges during warm weather more than other foundations and usually be used widely in the world. Ultimate capacity of piles is assessed by consideration of adfreeze strengths. A design based on settlement must ensure that pile displacements throughout the life of the structure are tolerable. So a lot of field load experiments have been carried out (Wang et al., 2005; Guo and Li, 2002; Zhang, 2002; Li et al., 2002) because prior experience with laboratory testing and field loading testing of permafrost is quite limited. These publications mainly considered the interaction mechanism between pile and permafrost, influence factors of the frozen strength, actual vertical bearing capacity measurement of pile and so on.

To meet the needs of the pipeline and housing construction in permafrost regions, the smaller diameter steel piles in North American countries had been studied primarily (Wu, 2003; Liu et al., 2002; Wang et al., 2003; Wu, 2003; Ma, 2003). Large diameter reinforced concrete piles had been seen seldom in permafrost regions of Russia although pile foundation is widely used in Russia. Model tests had been carried out to study the main factors of the frozen force in order to know the general rule that the freeze force influenced on temperature, moisture, soil particles on the freeze force (Crowther, 2013; Gang et al., 2013). Afterward, constructed buildings in Qinghai-Tibet plateau and Northeast of China requires specific knowledge about permafrost and specialized building techniques. The field loading testing the piles of house had been carried out in cold region of China northeast. It also meets constructing railways in Daxinanling. The pile testing ground had been set up specially to use for the static loading test and studying construction technology in permafrost region of Qinghai-Tibet plateau to meet the highway and railway constructions. However, so far the testing piles in permafrost have less than 0.65 m diameter and less than 8 m length. The testing piles have no means to meet the Qinghai-Tibet railway construction. Therefore, in order to know the formation law of bearing capacity of bored piles induced by the ground temperature change after bridge pile construction, the interaction between pile and soil around the pile must be carefully studied on conditions of field loading testing when the frozen soil refreezes. The transfer process of shaft force, pile lateral resistance and pile tip resistance must also be considered. The bearing experiment of bored pile in permafrost region of Qinghai-Tibet plateau will be used for the design and construction of railway.

IN SITU TEST

Ground temperature test hole was drilled at the southern Basin site of Beiluhe in Fenghuoshan Region between the Hoh Xil and Fenghuo Mountain on September 1, 2001 from Figure 1. It can be shown from Figure 2 that the site was found to be underlain by brownish red sandy soil, a fine-grained partly gritty soils, for example, angular gravel, detritus to a depth of about 0.7 m. At a depth of 0.7 m, a 3.3 m thick layer of brownish red clay, a massive ground-ice including soil, was present continuously across the site, and this layer was underlain again in turn by intense-weathered mudstone and sandstone, respectively at depths of 4 and 15.5 m, respectively below natural ground surface.

The measured temperatures on disturbed samples were obtained from test hole and some of the early hole for pile installation was highly variable from Figure 2. The sedimentary in the construction area are mainly lacustrine

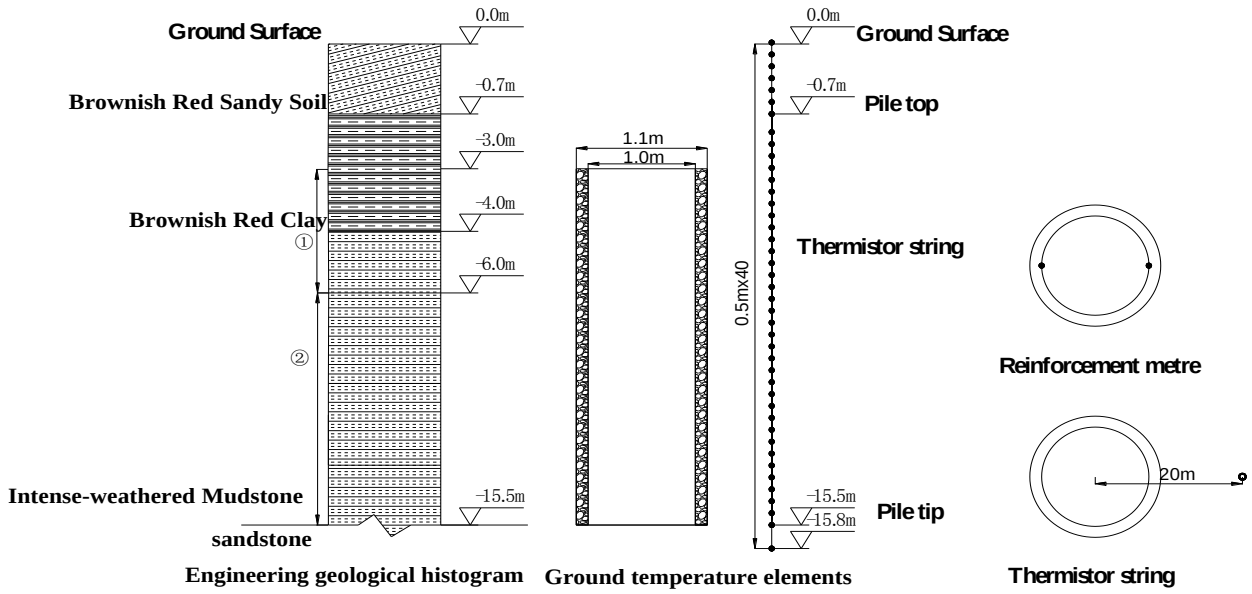

Figure 2. Geological columns, monitoring point arrangement and ground temperature elements.

sediments of tertiary and alluvial layer in holocene of quaternary. Massive ground-ice containing soils occur below the table with a typical thickness of 1 to 2 m. Ice-saturated and ice-rich soils are formed below the ice layers. According to the observed data from 2001 to 2002 in Figure 3, the mean annual air temperature in the region is -3.8°C and means annual ground temperature at a depth of 15.0 m ranges between -1.6 and -0.9°C, respectively. The annual ground temperature over most of the experimental site lies below -1.0°C. According to the permafrost site division theory based on ground temperature in China, the district is considered as basically stable with low temperature. And it belongs to the area of thick layer underground-ice in permafrost regions (JGJ118, 2011). It also is the arid climate zone and the freeze period as long as 7 to 8 months every year. At the site, the strata consist predominantly of lacustrine deposits of the upper Tertiary and diluvium of the Quaternary Holocene Series, such as silty clay. The permafrost table averages 2.0 to 2.5 m deep, but ranges up to 2.8 m deep.

Permafrost is an excellent foundation as long as it remains frozen. But it is very sensitive to temperature changes. Changes to the ground surface, for example, removing the ground cover or constructing will change the ground temperature and cause the permafrost to thaw and possibly lose its rigidity. A bridge radically changes the way heat moves in and out of the soil; and constructing a bridge on a permafrost site will affect the permafrost. Bridges are normally heated in the construction and this will add heat to the soil. A bridge also shades the soil in the summer, preventing exposure to the sun. So, the soil is warm in the winter when it should be cold, and cold in the summer when it should be warm. And every attempt is made to keep the soil beneath the bridge frozen and the permafrost stable. The strategy for alleviating the engineering risks of bridge on permafrost sites is to build the structure on piles or an elevated foundation, taking special care to insulate the ground and prevent thawing.

After general site conditions are evaluated, a more detailed investigation is normally required at the specific construction site. Structure of pile can be selected when there is permafrost present. Perennial freezing on well-drained, coarse-grained river sand and gravel or bedrock can be ignored because it has few associated problems. But in the permafrost zone, particularly with fine-grained soils with high ice content, every effort must be made to preserve frozen conditions. For some types of structures, it may not be possible to prevent thawing without special design considerations. However, the piles were widely used because the piles should be well embedded in the permafrost and the structure rose above the ground to permit natural air circulation beneath the structure and to minimize heat flow from the structure to the frozen ground. Piles are also driven in place with a pile driver. Therefore, the permafrost must be thawed with a steam jet while the bored pile can be constructed by drilling not by a steam jet. On the contrary, the permafrost can seldom be thawed when the bored pile can be drilled. Some permafrost around the pile can be thawed only after the concrete are poured into the drill. But the thawed permafrost would restore the original frozen state after refreezing. And the refreezing of the thawed permafrost around the pile would also increase the depth, stability and amount of permafrost and for stabilization during cold weather.

In addition, building foundations should be designed

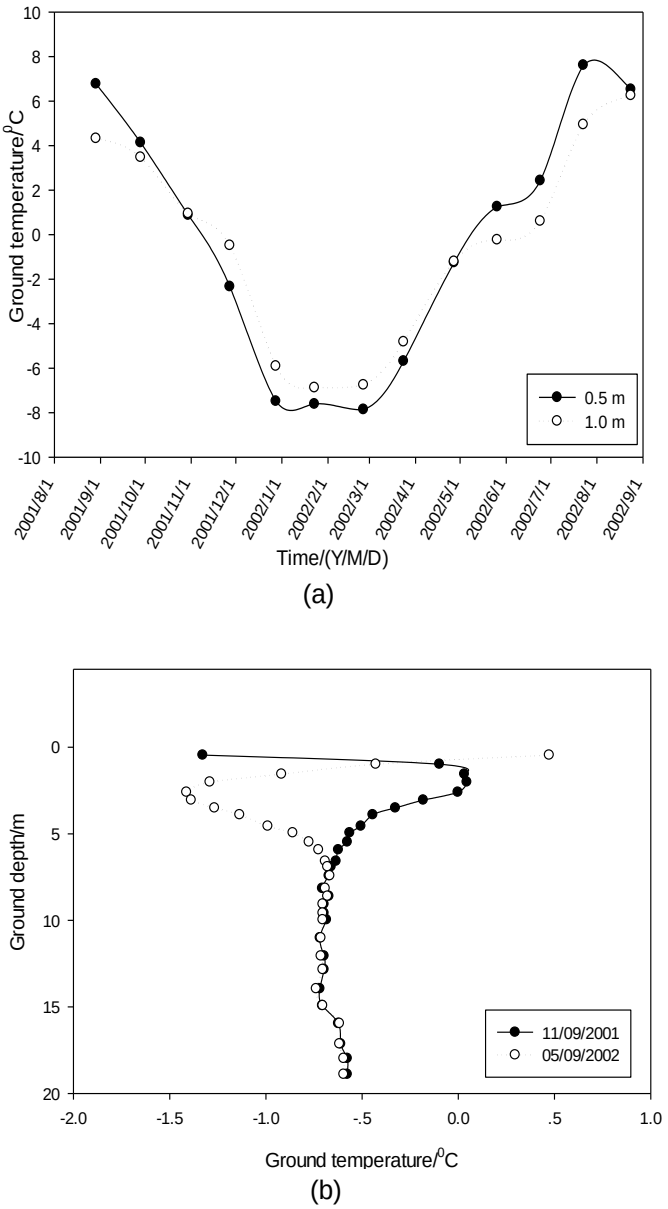

Figure 3. Ground temperature (a) at the depth of 0.5 and 1.0 m versus time and (b) at the depth of 0 to 20 m.

with a uniform weight distribution considering heaving action and thawing settlement; for example, lightly-loaded, improperly anchored piles may be pushed out of permafrost by the active layer and heaving action while the bored pile was considered as a uniform weight distribution preventing from be pushed out of permafrost by the active layer and heaving action. So the bored piles were widely used in the Qinghai-Tibet railway. In the permafrost region of Qinghai-Tibet, the diameter of railway test pile is designed as 1.0 m, and the embedded length is 12.5 m. It belongs to the large diameter bored pile according to the Technical Code for Building Pile Foundations of China (JGJ118, 2011).

MATERIALS AND METHODS

Pile placement

Based on a review of published information at the time of installation on permafrost properties and pile load capacities in such a material, it was considered that significant uncertainties were present concerning pile design in frozen ground. So it was decided to carry out a limited program of pile load testing to confirm or modify some preliminary estimates of pile load capacities. Owing to the short construction period available for foundation construction, and the requirement to complete the piling in the first construction season, piling operations were already underway before pile testing was started. Ground temperature of frozen soil surrounding the pile measurements were obtained during the pile testing program from 25 thermistor strings installed on September 28, 2011. Readings at subsequent dates are shown plotted in Figure 3a. It is observed that all thermistor strings were installed about 1 m away from the axis of test pile. The measuring hole installing thermistor strings had a depth of 15 m. The distance between two thermistor strings is 0.5 m. The readings indicate that the thawed active layer extended to about 8 m below ground surface.

To measure the shaft force of test pile, side resistance and tip resistance of pile, the 25 steel instruments were installed symmetrically inside a concrete-filled test pile. The distance between two steel bar meters is 0.5 m. Test pile had been constructed by the underwater perfusion concrete method (JGJ118, 2011). Separate posts were embedded into the permafrost to act as displacement gage supports. Two displacement gages accurate to 0.001 mm were mounted on the posts in such a way as to measure the settlement of the crossbeam on either side of the point of load application. The displacement gage readings were then averaged to obtain the settlement of the pile head. Survey levels of the pile heads were also taken from time to time to confirm the overall accuracy of the pile settlement monitoring as recorded by the displacement gages. Test pile began to be constructed on November 27, 2001. Drill of bridge piles was completed by the percussion drill. And steel cage was welded at the bridge site. The poured concrete was mixed near the concrete batching plant. Temperature of concrete varied from 1 to 3°C when poured into the mold. And test pile was completed on the end of December, 2001.

Loading method

Loading system consists of anchor pile, reaction beam and jack as shown in Figure 4. A steel crossbeam was fabricated, and was welded to four adjacent piles for each pile load test. Separate posts were embedded into the permafrost to act as dial gauge supports. Four dial gauges accurate to 0.025 mm were mounted on the posts in such a way as to measure the settlement of the crossbeam on either side of the point of load application. The dial gauge readings were then averaged to obtain the settlement of the pile head. Survey levels of the pile heads were also taken from time to time to confirm the overall accuracy of the pile settlement monitoring as recorded by the dial gauges. Considering the static loading test of pile in permafrost foundation and the experience of the foundation pile on the site on the Tibetan plateau carried out by Northwest Research Institute of Railways Ministry in the 1970s and 1980s and physical and mechanical properties of permafrost soil around the pile after soil mass refreezing, the fast loading method was used as loading of test pile. The main steps are as follows (JGJ118, 2011).

Load classification

Load was applied by a 600 kN hydraulic jack. The jack was calibrated before and after the test program to ensure accuracy of

Figure 4. Field pile loading test.

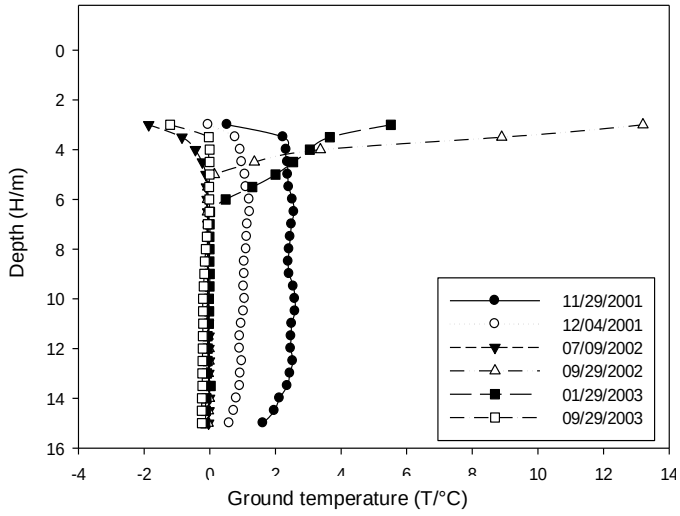

Figure 5. Curve of ground temperature around pile.

the load application system. Considerable fluctuations in the applied jack load occurred during the test pile, and steps were taken to reduce these fluctuations in subsequent load tests. According to the estimated ultimate bearing capacity of test pile, the load level is divided into 10 levels. Load was applied by a 600 kN hydraulic jack between 1 and 6 and between 9 and 10. Other load was applied by a 400 kN hydraulic jack. The settlement of the pile top is less than 0.1 mm every hour, or settlement rate of test pile is less than 0.1 mm/h under each level of loading. However, the settlement of testing pile has been considered to be stable under the loading level if the sedimentation rate of continuous observed average settlement in half-hour appears three times. The field loading test can be terminated when the settlement test pile accelerated or its total settlement of pile block is more than 40 mm. Considerable fluctuations in the applied jack load (up to 10% of the applied 600 kN load) occurred during the test pile, and steps were taken to reduce these fluctuations in subsequent load tests. The unloading value is as much as 2 times of loading value.

Frequency readings

During normal working periods, readings were generally taken once separately every 5, 15, 40 min during each stage of loading, and during night time periods, every 4 to 8 h. Afterwards, loading is measured once every one hour. Loading is measured once every 30 min when loading is close to the bearing capacity of the pile. Ground temperature of permafrost around the pile was observed once every 24 h. This reading schedule was continued for the duration of each test, which continued for 3 to 7 days.

RESULTS AND DISCUSSION

Refreezing analysis process of testing pile side surface

Readings at six subsequent dates are shown plotted in Figure 5. The readings indicate that the thawed active layer extended to about 0 to 3 m below ground surface. The ground temperature around test pile within 0 to 3 m under natural ground surface is not considered when the thawed frozen soil induced by construction refreezes. The reason is that the ground around test pile within 0 to 3 m under natural ground surface had been often excavated and exposed. The natural ground surface within 0 to 3 m also had no influences on the bearing capacity of test pile. The ground temperature around test pile within 0 to 3 m under natural ground surface has little significance for the bearing capacity of test pile. Therefore, the ground temperature around test pile only within 3 to 15.5 m under natural ground surface was considered.

As shown in Figure 2, the test pile is divided into two parts to analyze ground temperature below test pile top because the ultimate bearing capacity was related closely with the active depth of permafrost. The first part was marked as ① where it was -3 from -6 m below natural ground surface. The second part was marked as ② where it was beyond -6 m below natural ground surface. Figure 3 showed that ground temperature below the ground surface had been basically less than 0°C after November 1, 2001 at the depth of 0.5 and 1.0 m, respectively. But ground temperature below the natural ground surface had been under 0°C except within 0 to 3 m under natural ground surface.

According to the arrangement of reinforcement meter and the measured frequency, the following shaft force of pile formula was calculated by the pile concrete strain data.

$$Q_i = A_p \sigma(\varepsilon_i) \quad (1)$$

Where: Q_i is pile shaft force under the loading level I; A_p is the cross-sectional area of pile; ε_i is the pile concrete strain under the loading level i.

Pile side freezing force or pile side resistance of each layer soil is calculated by the following equation:

$$f_i = (Q_i - Q_{i-1}) / A_p \quad (2)$$

Pile tip resistance is calculated by the following equation:

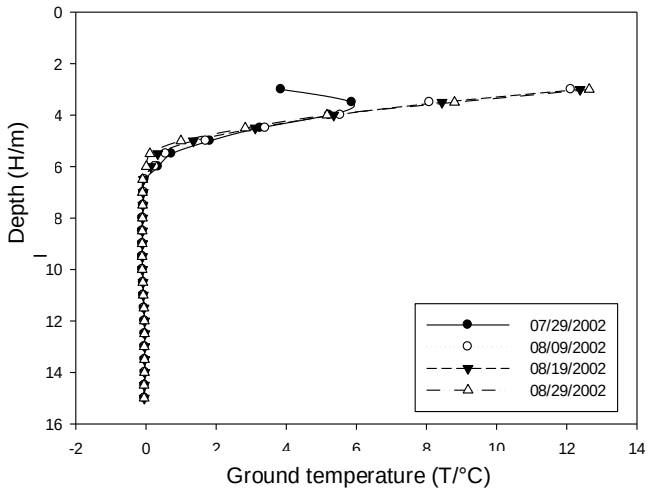

Figure 6. Ground temperature curve of pile's wall during loading.

$$Q_b = Q_{up} / A_p \quad (3)$$

Where: Q_{up} is pile tip resistance.

Figure 5 presented the curved temperature profile below this elevation which is typical of a late-winter temperature profile in a continuous permafrost zone. It can be seen that the ground temperature of all measured points around the test pile wall had a sharp increase due to absorption of concrete hydration heat and became higher than 0°C after the pile hole had been just poured into concrete which varied from 1 to 3°C on November 27, 2001. The measured maximum temperature even reached 13°C on the pile top because of the hydration heat of concrete releasing. Subsequently, the overall measured ground temperature around the test pile wall began to decrease and dropped to 2°C or so 3 days after the pile had been completed. The ground temperature only at a depth of 3.5 m under the pile top still dropped to -0.025°C 25 days after the pile had been completed and this provides an estimate of the average annual ground temperature at the site. The ground temperature of all measured points around the test pile wall was below 0°C 103 days after the pile had been completed on September 29, 2003. Bored-pile directly could be bonded with hole-wall in permafrost as long as the ground temperature around test pile was below 0°C. So the shear strength of the interface between pile and soil was enhanced. The bearing capacity of the pile can be improved. The bearing capacity of the pile had almost reached the maximum value at present and would be a stable state. The temperature below this elevation would not normally be expected to vary by more than 1°C or so throughout the year. The design poured depth of bored pile is from 3 m to 15.5 m under natural ground surface. The measured ground temperature 3 m below the natural ground surface would be analyzed carefully.

Besides, it is very essential for the bearing capacity of pile to analyze ground temperature change around pile when the thawed frozen soil induced by construction refreezes because the shear strength is a function of temperature. It demands more worthy attention especially during test pile loading. The measured ground temperature on the pile top was up to 13.2°C during loading of the test pile, as can be seen from the Figure 6. The ground temperature in the area of ① is always above 0°C, but the ground temperature in the area of ② is always below 0°C during loading of the test pile. And this is mainly caused by the warming climate and excavation of pile foundation pit of pile caps in bridge abutment. The measured ground temperature on the pile top had dropped to 3.85°C when loading of the test pile was completed. But the all measured ground temperature around the test pile wall were higher than before the test pile was loaded in despite being lower than 0°C. This was mainly caused by the external loading. In addition, permafrost is particularly insensitive to the outside temperature when the ground temperature is near 0°C.

The above studies show that the ground temperature around the test pile was higher than before test pile was not excavated because the ground was disturbed by the construction and the weather outside. After this period, it was difficult to recover the original ground temperature. The ground temperature in the area of ① is always above 0°C, but the ground temperature in the area of ② is always below 0°C during loading of the test pile. Therefore, there was no freezing force in the pile side surface in the area of ① but there was freezing force in the pile side surface in the area of ②.

Bearing characteristics of testing pile

Figure 7 presented the results for settlement on pile top against load on pile top for test pile. Steep drop P-S curve of test pile indicates that test pile is nearly close to pure friction pile because the soil on the end of the test pile is sandstone with lower strength and high compression, as shown in Figure 2. It is also seen from Figure 7 that the loading-settlement process of test pile can be divided into three stages based on the elastic-plastic deformation of permafrost around pile. They are respectively elastic (OA), elastic-plastic (AB) and plastic (BC) in Figure 7.

(Elastic stage OA (0 to 2400 kN)

As can be seen from Figure 6, the ground temperature where it was 3 to 6 m below test pile top is always above 0°C, but the ground temperature within 6 to 15.5 m below test pile top is always below 0°C at the beginning of test pile loading. And there was no freezing force on the pile side surface 3 to 6 m below test pile top but there was freezing force on the pile side surface within 6 to 15.5 m

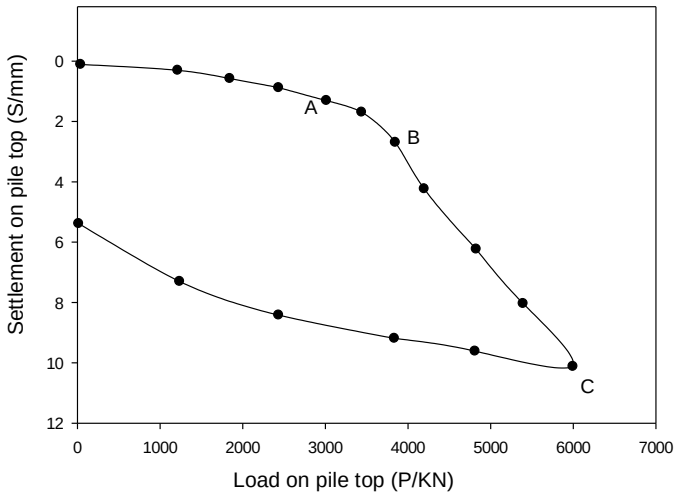

Figure 7. P-S curve of pile.

below test pile top. The pile length below 0°C is far more than over 0°C. Load ground transfer along the pile was undertaken by pile side resistance because freezing force on the pile side surface was far more than pile side resistance. With the pile loading increasing little by little, the pile side resistance was also increasing. At present, pile tip resistance also has a small increase. The ground temperature in the area of ① is always above 0°C during loading of the test pile. So there is no freezing force on the pile side surface in the area of ①. The ultimate value of pile side resistance is less than the ground temperature in the area of ① which is always below 0°C. A of P-S curve appears earlier than the ground temperature in the area of ① which is always below 0°C. The elastic deformation duration of soil around test pile is relatively short. However, both freezing force on the pile side surface and pile side resistance had always been less than the shear strength of ground within the static loading of 0 to 2400 kN. The permafrost did not appear as shear failure although the shear deformation zone of frozen soil around test piles expanded to the surrounding continuously.

Elastic-plastic AB (2400 to 3800 kN)

Ground around the test pile begin to appear as plastic deformation because pile side resistance in the area of ① began to be more than the shear strength of ground when the static loading was beyond 2400 kN. But both freezing force on the pile side surface and pile side resistance in the area of ② had been less than the shear strength of permafrost. So the permafrost in the area of ② did not appear as shear failure although the static loading had already reached 2400 kN. The shear deformation zone of frozen soil around test piles continued expanding to the surrounding continuously with the static loading. Pile side resistance begins to extend down from test pile top along the pile. Meanwhile, the plastic-deformation of the soil around test pile begins to expand downward permafrost gradually. Pile side resistance along the pile reaches the limit value when the plastic zone extends from the top of test pile to the end of the pile until the static loading reached 3800 kN. Pile side resistance was unable to withstand the increased loading again from test pile top. Both freezing force on the pile side surface and pile side resistance had been more than the shear strength of ground when the static loading reached 3800 kN. The pile tip resistance of test pile begins to bear the increased load again if the static loading continued increasing. Due to the large diameter and the short length of bored piles, and the low strength of sandstone at the pile tip, the curvature of the curve AB is relatively large and duration time of elastic-plastic deformation of the frozen soil around the pile is very short.

Plastic stage BC (3800 to 6000 kN)

The plastic deformation of permafrost around pile would persist for a long time due to the irreversible shear effect of particles and particle aggregating in permafrost causing visco-plastic flowing deformation. The sedimentation rate of test pile is relatively slow as shown from Figure 8. The settlement on the pile top have a sharp increase; the settlement rate is accelerated too, and the curves of S-lg t appear polyline and have a sharp increase in the slope of the curve when the load capacity reaches 6000 kN on the top of the pile. It can be speculated that 6000 kN is ultimate bearing load capacity of the test pile. Under this load, the total settlement of pile is 10.15 mm. The residual settlement of test pile is 5.53 mm after unloading. Rebounding rate of test pile was 58.48%. The load-settlement characters of test pile show a typical characteristic of a friction pile. The total settlement of the test pile in the elastic and elastic-plastic stages is 8.74 mm known from the load-settlement process of test pile. And the settlement in the plastic stage is 7.41 mm. So the deformation of permafrost around test pile is mostly plastic deformation from pile top to pile tip. The load-settlement characteristic of test pile also shows characteristics “L” of a typical friction pile. In addition, thawing and refreezing of permafrost around test pile are caused by cement hardening and its temperature after the pouring of concrete in permafrost regions.

In addition to the mortar infiltration into soil around test pile, test pile bonding directly with pile wall can improve the bearing capacity of pile greatly. However, it was affected by the excavation of foundation pit before loading on the test pile. There is only frozen force on the pile side surface in the area of ②. The bearing capacity of test pile has not been fully realized.

Therefore, the pile at this site appeared to be incapable

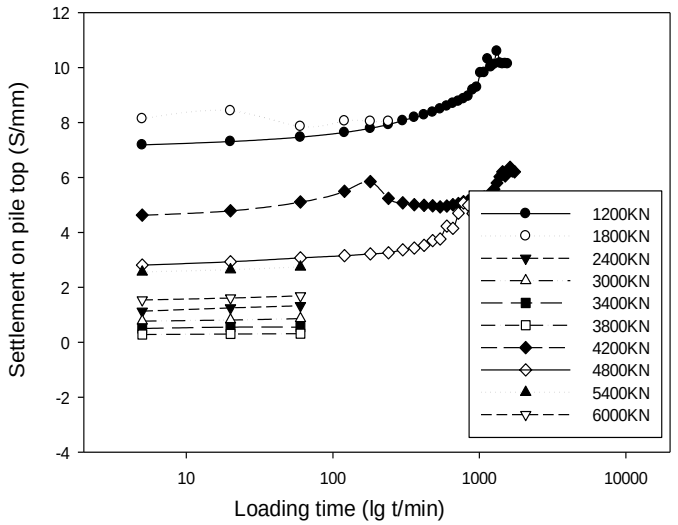

Figure 8. S-lgt curve of pile.

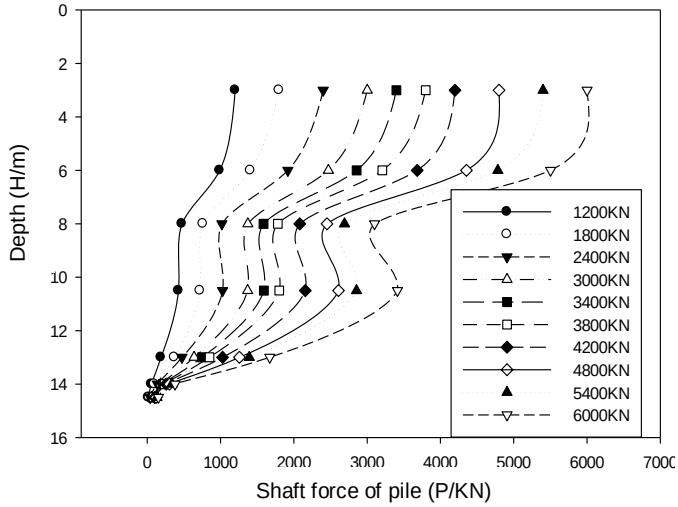

Figure 9. curve of pile shaft force with different load.

of supporting pile-shaft ultimate load in excess of about 6000 kN for the ground-temperature conditions prevalent during the test in the broadest sense. At a load level of 6000 kN, one test pile showed very high settlement rates immediately after load application. These pile capacities are quite low, even for piles in contact with icy permafrost. These findings prompted the designers to introduce other methods of foundation cooling in order to increase the allowable pile load capacities for the building. Allowable pile side stresses in permafrost would normally have been expected to be in the range of 407.19 kPa for these ground temperature conditions based on the above experience and theoretical considerations. The influence of rich-ice, and possibly also of pile installation method, have obviously introduced major reductions in pile capacity.

Load transfer characteristics of test pile side

Figure 9 presented curve of pile shaft force with different load. And curve of pile side resistance with different load is given in Figure 10. The pile shaft force and pile side resistance around test pile can be calculated according to the measuring values of steel instruments under different load conditions. Figure 9 shows that the pile shaft force along the test pile decays gradually under different loads. The pile tip resistance is very small and the increase of the pile tip resistance is slow relatively. It indicates that the vertical load on the pile top is balanced by the pile side resistance coming from the soil around test pile. With the increase of load on the top of pile, the attenuation trend of pile shaft force along test pile presents accelerating gradually. It is more obvious especially 0 to 10.5 m below the pile top. The attenuation trend of pile shaft force at the different depth is different even though under the same load. This may be related to the character of permafrost around test pile. For example, when the shaft force of test pile is loaded to 3200 kN, the attenuation trend of pile shaft force in strongly weathered marl layer 3 to 5 m below the top of test pile is significantly faster than intermediary weathered 7.5 to 10.5 m below the top of test pile. The attenuation trend of pile shaft force is relatively flat when load on the pile top is small. This is caused by the smaller deformation of the pile cross-section and pile side resistance not fully developing. There is a larger gradient change pile shaft force 3 to 5 m, 5 to 7.5 m and 7.5 to 10.5 m below the pile top, respectively. And the corresponding pile side resistance is larger, too. On the contrary, there is a smaller gradient change pile shaft force 0 to 3 m and 10.5 to 12.5 m below the pile top, respectively. And the corresponding pile side resistance is smaller, too.

It is seen from Figures 10 that the pile side resistance increases with the increasing of loading in the same soil. And there are limit value of pile side resistance within 3 to 7.5 m and 7.5 to 11 m below the pile top under every load level. The limit value of pile side resistance within 3 to 7.5 m and 7.5 to 11 m below the pile top were separately 378.39 and 407.19 kPa, respectively when loading reached 6000 kN. From the view of geological data, the geologies within 3 to 7.5 m and 7.5 to 11 m below the pile top were separately strongly weathered marl layer and intermediary weathered marl layers. According to the ground temperature at that time, the strongly weathered marl layer within 3 to 7.5 m below the pile top had so higher ground temperature that the pile side resistance was extremely small. The intermediary weathered marl layer within 7.5 to 11 m below the pile top had lower ground temperature. So the pile side resistance was extremely great. These should be related with the ground temperature.

Curve of the pile side resistance varied with load under

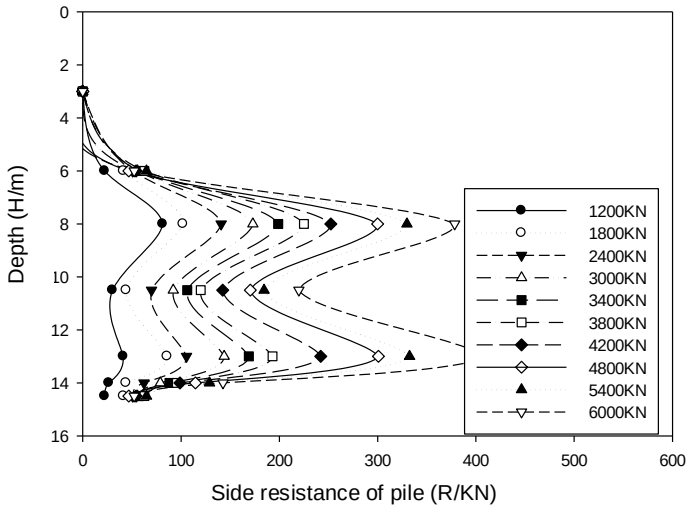

Figure 10. Curve of pile side resistance with different load.

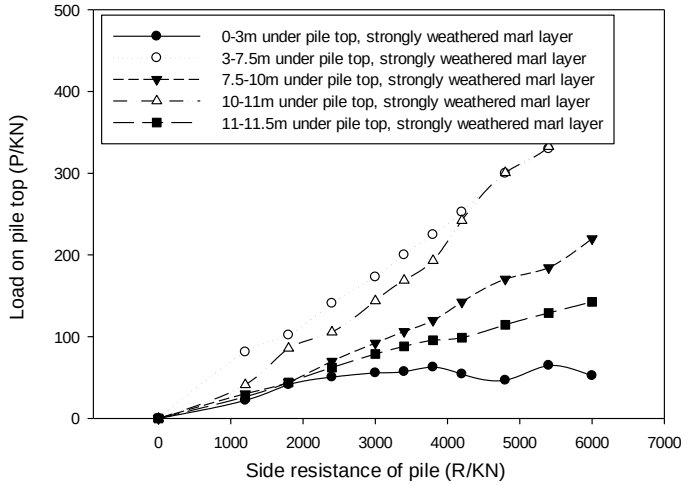

Figure 11. Pile side resistance curve of different soil layer with loading.

the different layers, as shown in Figure 11. Except for soil between within 0 to 3 m below the pile top, pile side resistance presented a linear increase with load on the pile top before loading reached the ultimate load 6000 kN. The increase of pile side resistance in the strongly weathered marl is the fastest within 3 to 5 m below the pile top. This may be related to the strongly weathered marl with a temperature always below 0°C. But the pile side resistance in strongly weathered marl layer had almost no any increasing within 0 to 3 m below the pile top. It indicated that the soil around test pile within 0 to 3 m below the pile top had reached the limit prior to other soil. This is because the strongly weathered marl within 0 to 3 m below the pile top had a temperature always over 0°C. In addition, pile tip resistance and loading sharing ratio of pile tip resistance increase with load on the pile top, as shown from Table 1. Load sharing ratio of pile tip resistance almost had no increase when the load increased from 4800 to 6000 kN, respectively. It also indicated that the load on the pile top is mainly borne by the pile side resistance.

Influencing factors analysis of testing pile bearing

It is not difficult to speculate from the above analysis that the primary unknown in this performance analysis involves the properties and behavior of the frozen-back permafrost around test pile. If competent bedrock is within practical piling distance of the ground surface then end-bearing pile is preferred. In fact, friction pile is preferred because competent weathered marl is within practical piling distance of the ground surface. The frozen soil around test pile will have adequate bearing capacity because of freezing force of pile side if the ground temperature below test pile top is always below 0°C. If this approach is either impractical or impossible then the piles must develop adequate bearing capacity in frozen or unfrozen soils. Permafrost is insensitive to the outside temperature when the ground temperature is near 0°C. Settlement and strength properties of warm frozen soils (greater than 0°C) are still poorly defined. Moreover, the thermal regime of such soils is in a delicate state of equilibrium. Therefore it is recommended that the pile foundation be determined only for the length of the pile bored in permafrost colder than 0°C. Consequently, in marginal permafrost areas where the ground temperature is warmer than 0°C, special precautions must be taken. If the permafrost is thaw-stable then the design may be based on the unfrozen soil properties. If the permafrost is thaw unstable then the soil may be pre-thawed and compacted. The warm frozen soil temperature must be lowered using artificial refrigeration to keep the stability of pile foundation in permafrost. Pile design is then identical to that for cold permafrost. For a friction pile the allowable pile load is determined from both settlement and strength considerations.

However, some studies only considered the ultimate bearing capacity of pile under disturbed permafrost not the original undisturbed state (Wang et al., 2013). It means that the ultimate bearing capacity of pile does not fully play although the pile has a high vertical bearing capacity and a small deformation under a non-fully refreezing condition. So the ultimate bearing capacity of pile must be considering a fully refreezing condition.

The allowable adfreeze strength may be estimated from Figures 9 and 10. It is emphasized that the allowable adfreeze strength must consider the soil condition at the pile interface during test pile loading. Thus, for the bored pile poured in winter, the moisture migration to the pile during freeze back will result in an ice lens at the pile-soil interface and therefore the allowable adfreeze strength should be equal to that of a

Table 1. Loading sharing ratio of pile tip resistance.

Load levels/kN	1200	1800	2400	3000	3400	3800	4200	4800	5400	6000
Pile tip resistance /kN	15.83	26.37	39.55	58	71.17	84.33	102.75	121.17	131.68	152.78
Load sharing ratio/%	1.3	1.5	1.6	1.9	2.0	2.2	2.4	2.5	2.4	2.5

pile in ice. Further, the adfreeze strength must be determined for the warmest soil conditions throughout the design life. In order to satisfy settlement criteria in ice-poor soils it is necessary to determine the flow law parameters. The approaches are almost certainly conservative but this should not preclude the application of a factor of safety. It is recommended that the safety factor be applied to the bored area. Its magnitude will depend upon the construction control and, more importantly, the accuracy of the soil property values used in the analysis. Finally it is noted that the net allowable structure load per pile is equal to the allowable axial pile load as determined from the down drag loads within the active layer. The in-situ ground temperature tests and static loading tests were used for the pile foundation design of the Qingshuihe Bridge located at the Qinghai-Tibet railway during its construction.

Conclusions

From the aforementioned results and analyses, we can find several significant conclusions for bearing characteristics and influencing factors analysis of bored pile under refreezing condition in permafrost region.

(1) It is as far as possible to avoid disturb permafrost by construction when the bored pile is constructed in the unstable underground thick ice layer of high temperature permafrost region. It is very difficult to recovery once permafrost is disturbed.
(2) The load-settlement process can be divided into three stages based on P-S curve of the field loading test. They are separately elastic, elastic-plastic and plastic. So the deformation development process of frozen soil of pile side and the interaction process between pile and pile side soil is analyzed.
(3) Pile tip resistance accounted for the entire load is just 2.5% when load on pile top reached 6000 kN. Pile tip resistance is not too important for the bearing capacity of test pile.
(4) The test result of shaft force and pile side resistance indicate that the attenuation characteristics of shaft force and distribution of pile side resistance along test pile is closely related to the load on the pile top, the properties of permafrost around test pile and ground temperature.

ACKNOWLEDGEMENTS

This paper was supported by State Key Laboratory for GeoMechanics and Deep Underground Engineering, China University of Mining and Technology, the Young Teacher Training Program of Southwest Petroleum University, and Rock and Soil Mechanics and Engineering Scientific Research Innovation team of Southwest Petroleum University, No. 2013XJZT006.

Conflict of Interests

The authors have not declared any conflict of interests.

REFERENCES

Biggar KW, Kong V (2001). An analysis of long-term pile load tests in permafrost from the Short Range Radar site foundations. Can. Geotechn. J. 38(3):441-460. http://dx.doi.org/10.1139/t00-110
Crowther GS (2013). Frozen Soil Strength Criteria for Lateral Pile Analysis. J. Cold Regions Eng. 27(3):155-167. http://dx.doi.org/10.1061/(ASCE)CR.1943-5495.0000058
Gang QK, Qing Y, Han LL (2013). Numerical study of a new belled wedge pile type under different loading modes. Eur. J. Environ. Civil Eng. 17S:65-82.
Guo Y, Li J (2002). The construction of drilled poured in place pile in the ever-frozen soil area in Qingzang plateau. Chin. J. Shan-xin Architect. 28(2):35-36.
Li X, Zhang L, Zhang X (2002). A Summary of Testing Study on cast-in-place Bored Pile in Deep Iced Ground. Chin. J. China Railway Standard Des. 12:28-30.
Liu Z, Zhang Z, Zhang D (2002). Application analysis of Bridge Foundation in Permafrost Regions of the Qinghai-Tibet Railway, Chinese J. Sci. Technol. Intercommun. 32(4):17-19.
Ma T (2003). Construction Techniques of Bridge pile foundation in Ever-Frozen soil Areas for Qinghai-Tibet Railway. Chin. J. Bridge Constr. 2:53-54.
Niu Y, Liu Y (2004). Field observation on responses of soil temperature profile to construction of engineering piles in permafrost. Chin. J. Rail Eng. 81(1):30-33.
Suleiman, Muhannad T, Sritharan, SRI, White, David J (2006). Cyclic lateral load response of bridge column-foundation-soil systems in freezing conditions. J. Struct. Eng.-Asce. 132(11):1745-1754. http://dx.doi.org/10.1061/(ASCE)0733-9445(2006)132:11(1745)
The Professional Standards Compilation Group of People Republic of China (2011). The designing criterion of the foundations in permafrost regions. Beijing: China Architecture and Building Press, JGJ118.
Wang D, Fu Z, Fang J, Li H (2008). Influence of solar radiation on surface thermal regime of different pavement types and its permafrost underlying embankment on the Qinghai-Tibetan Plateau. J. Highway. Transport. Res. Dev. 25(3):38-43.
Wang X, Chen P, Wu S (2003). Study and Application of Pile Foundation in the Qinghai-Tibet Railways. Chin. J. Railway 1:66-88.
Wang X, Jiang D, Liu D (2013). Experimental study of bearing characteristics of large diameter cast-in-place bored pile under no refreezing condition in low temperature permafrost ground. Chin. J. Rock Mechan. Eng. 32(9):1807-1813.
Wang X, Jiang D, Zhao X (2005). Experimental study on bearing features of bored pile under non-refreezing condition in permafrost region. Chin. J. Geotechn. Eng. 27(1):81-84.
Wu S (2003). Problems in the cast-in-place Pile Foundation in

Permafrost Regions of the Qinghai-Tibet Railway. Chin. J. Glaciol. Geocryol. 25(S):59-68.
Xiuli D, Jianjun Z, Weiming Y, Yue L, Jianwei Z (2012). The Research of Pile Load Test on Permafrost Regions. Adv. Mater. Res. 446:1123-1126.
Yao Z, Huang X, Chen Z, Zhang J (2012). Comprehensive soaking tests on self-weight collapse loess with heavy section in Lanzhou region. Chin. J. Geotechn. Eng. 34(1):65-74.
Zhang J (2002). Study on Design and Construction of Bridge and Culvert in Secular Frozen Earth Area in Plateau. Chin. J. China Railway Sci. 12:28-30.
Zhang J, Ma W, Wang D, Yuan X (2008). In-situ experimental study of the bearing characteristics of cast-in-place bored pile in permafrost regions of the Tibetan Plateau. J. Glaciol. Geocryol. 30(3):483-487.
Zhu B, Li G (1982). Experimental study of pile foundation in permafrost region on Kunlun Mountains. Lanzhou: Northwest Institute, China Academy of Railway Sciences.

academicJournals

Vol. 9(14), pp. 645-651, 30 July, 2014
DOI: 10.5897/SRE2014.5895
Article Number: F21242846447
ISSN 1992-2248 © 2014

http://www.academicjournals.org/SRE

Scientific Research and Essays

Full Length Research Paper

Visualization analysis of feed forward neural network input contribution

Jamal Alsakran[1]*, Ali Rodan[1], Nouh Alhindawi[2] and Hossam Faris[1]

[1]The University of Jordan, Amman, Jordan.
[2]Jadara University, Irbid 21110, Jordan.

Received March 31, 2014; Accepted 1 July, 2014

The complexity of domain problem can slow or even hinder the learning process of neural networks. It is rather difficult to overcome such an obstacle because neural networks, as cited today in the literature, lack the interpretability of their internal structures. In this paper, we present a visualization approach capable of enhancing the understanding of neural networks. Our approach visualizes input and weight contributions, sensitivity analysis, and provides guidance in pruning less influential features and consequently reducing the complexity of domain problem while maintaining acceptable error rates. We conduct experiments on various datasets to show the effectiveness of our approach.

Key words: Neural network, visualization, input contribution, sensitivity analysis

INTRODUCTION

The human brain has the ability to perform multi-tasking. These tasks include controlling the human body temperature, blood pressure, heart rate, breathing, and other tasks that enable human beings to see, hear, smell and so on. The brain can perform at a rate that is far less than the rate at which the conventional computer can perform the same tasks (Haykin, 1999). Very little is known about how the brain actually works but there are computer models that try to simulate the same task that the brain carries out. These computer models are called *Artificial Neural Networks* (ANN), and the method by which the neural network is trained is called a *Learning Algorithm*, which has the duty of training the network and modifying weights in order to obtain a desired response.

Achieving a near optimal ANN for a specific problem requires a prior knowledge of the domain problem and an intelligent choice of network parameters such as weights, size of hidden layers, learning rate, etc. On the other hand, the lack of interpretability of the internal characteristics of a trained network hinders the construction of near optimal ANN (Sjöberg et al., 1995). Moreover, when the complexity of domain problem increases, reaching desired results becomes more difficult and unmanageable.

Reducing the complexity of domain problem by removing less influential features can ease the construction of desired ANN. However, as we do not have a good understanding of how neural networks work it is rather difficult to know which features available are the most useful in describing the key properties of the

*Corresponding author. E-mail: j.alsakran@ju.edu.jo

input vector class. Besides, manual pruning of domain problem is considered a tedious and error-prone task (Abraham, 2004).

Visualization can help understand complex systems (Viste and Skartveit, 2004). In this effort, we present a visualization approach to help understand input contributions and internal structures of multiclass feed forward neural networks. Our approach provides the necessary guidance, through means of visualization, to reduce the complexity of the problem, by pruning less important features, while achieving good results with acceptable errors. We attempt to visualize the knowledge learned by neural network such as input and weight contributions, sensitivity analysis. To the best of our knowledge, our visualization approach is the first to visualize input significance of multiclass output classification problems.

RELATED WORK

There has been much research devoted to studying sensitivity analysis and feature extraction of neural networks. Readers are referred to a comprehensive review and comparison of methods to study the contribution of input variables (Gevrey et al., 2003). Garson (1991) and Goh (1995) partition the connection weights to determine the relative importance of inputs. Milne (1995) proposes a modified version of Garson's method to determine input variable importance. Her calculation takes into account that weights can be positive or negative, and gives a better measure of contribution of inputs to outputs. Numerical sensitivity analysis is proposed in Montao and Palmer (2003) to interpret the effect of input variables on output without making an assumption about the nature of the data. More recently, Paliwal and Kumar (2011) propose a method based on the interquartile range of the distribution of the network weights obtained from training the network. They have shown that their method performs better than the connection weight approach proposed by Olden and Jackson (2002).

Visualization of the structure and behavior of neural networks has witnessed some research attention. Fischer and Zell (2000) develop an interactive visualization tool to help gain insights into neural network architectures and how the learning progresses and knowledge are stored in a network. Steeler et al. (2001) describe an interactive tool used to examine the weights and topology of neural networks. An evolutionary adaptation process is used in their tool to allow weights to be adjusted during training. They also present a compact matrix representation allowing many neural networks to be compared and organized in a tree structure. In the work presented by Tzeng and Ma (2005), the significance of input units and connection weights is mapped to color-coded units and edges of varying size, respectively. Their work merely visualizes one output class classification tasks while in our work we deal with multiclass classification tasks. Moreover, we visualize input contribution and sensitivity analysis in pursuit of better understanding of data features and reducing the complexity of the domain problem.

ARTIFICIAL NEURAL NETWORKS

Feedforward Neural Network (FFNN) model is called a multilayer perceptron network that consists of input, hidden, and output layers. Let a FFNN with K input units, N hidden units, and L output units, where $s = (s^1, s^2,\ldots,s^K)^T$, $x = (x^1, x^2,\ldots,x^N)^T$, and $y = (y^1, y^2,\ldots,y^L)^T$, are the inputs of the input nodes, the outputs of the hidden nodes, and outputs of the output nodes, respectively. A three-layer FFNN is shown in Figure 1. In FFNN, all the network weights are assigned random values initially, and the goal of the training is to find the set of network weights that causes the output of the network to match the teacher values as closely as possible.

Input contribution

As proposed by Garson (Garson, 1991), input contribution measures the influence of input towards output class. Input that has large contribution carries essential features of the data. We adopt a modified version of Garson's which is proposed by (Milne, 1995) because it takes into account that weights could be negative or positive. Contribution of input i to output l is computed as follows:

$$\frac{\sum_{n=1}^{N} \frac{w_{in}}{\sum_{k=1}^{K}|w_{kn}|} w_{nl}}{\sum_{k=1}^{K}\left(\sum_{n=1}^{N}\left|\frac{w_{in}}{\sum_{k=1}^{K}|w_{kn}|} w_{nl}\right|\right)} \quad (1)$$

where, in general, w_{xy} represents the weight between unit x in layer n and unit y in layer $n + 1$.

Input that has a contribution close to zero can be excluded from training. A large positive contribution of input towards an output favors that output class while a large negative value tends to favor other output classes.

Weight contribution

The knowledge learned by the neural network is internally stored in the network weights. Thus, it is critical to measure the positive or negative contribution of those weights. For hidden-output weights, we measure the contribution by the value of weight they hold when the training process is done as follows:

$$C_{nl} = w_{nl} \quad (2)$$

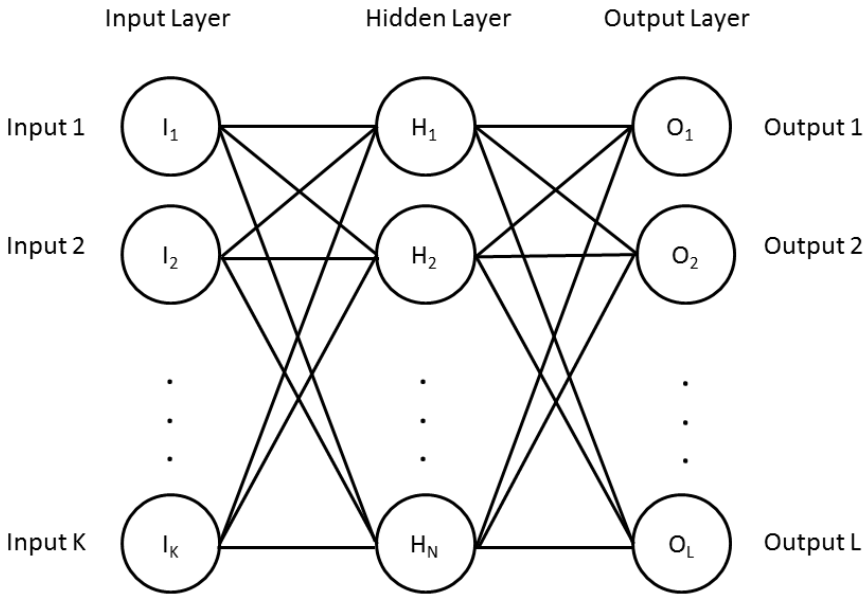

Figure 1. An example of the topology of a three-layer feedforward neural network.

In FFNN, the error propagates back between the current output and target output in order to modify the weights. Therefore, in measuring input-hidden weight contributions we propagate the layers influenced by multiplying the weights between input-hidden by all hidden-output weights connected to them as follows:

$$C_{kn} = w_{kn} \sum_{l=1}^{L} w_{nl} \quad (3)$$

Sensitivity analysis

Sensitivity analysis measures the effect that changes in input I_k have on output O_l. The effect indicates the significance of input on class output. Sensitivity analysis is calculated by taking the partial derivatives of input I_k with respect to output O_l (Montao and Palmer, 2003; Engelbrecht and Cloete, 1998) as follows:

$$\frac{\partial o_l}{\partial i_k} = o_l(1-o_l) \sum_{n=1}^{N} w_{nl} y_n (1-y_n) w_{kn} \quad (4)$$

Where y_n is a hidden unit activation, w_{nl} is the weight between hidden n and output l, and w_{kn} is the weight between input unit k and hidden unit n.

The sensitivity depends on information learned by the neural network, which is stored in w_{nl} and w_{kn}, and also depends upon the activation of the neurons in the hidden and output layers. In Equation 4, different input patterns p (input vectors) can provide different values for the change of effect. Thus, the sensitivity S is measured by taking the maximum effect to output due to a change in input as follows:

$$S_{ik} = \max_{k=1,\ldots,K} \sqrt{\frac{\sum_{p=1}^{P} \left[\frac{\partial o_l}{\partial i_k}\right]^2}{P}} \quad (5)$$

where P is the number of input patterns (or input vectors in the data).

Similarly, sensitivity is calculated for hidden units, input-hidden weights, and hidden-output weights as shown in Equations 6, 7 and 8, respectively.

$$\frac{\partial o_l}{\partial y_n} = o_l(1-o_l) w_{nl} \quad (6)$$

$$\frac{\partial o_l}{\partial w_{nl}} = o_l(1-o_l) y_n \quad (7)$$

$$\frac{\partial o_l}{\partial w_{kn}} = o_l(1-o_l) w_{nl} y_n (1-y_n) i_k \quad (8)$$

NEURAL NETWORK VISUALIZATION

In designing our visualization approach, we opt to preserve the familiar structure of neural network so that understanding our visualization would come natural to anybody who has been exposed to neural network structure. We choose to visualize input, hidden, and output units as round shapes, and weights as edges connecting those round shapes.

Input contribution visualization

Figure 2 shows an example of input contribution

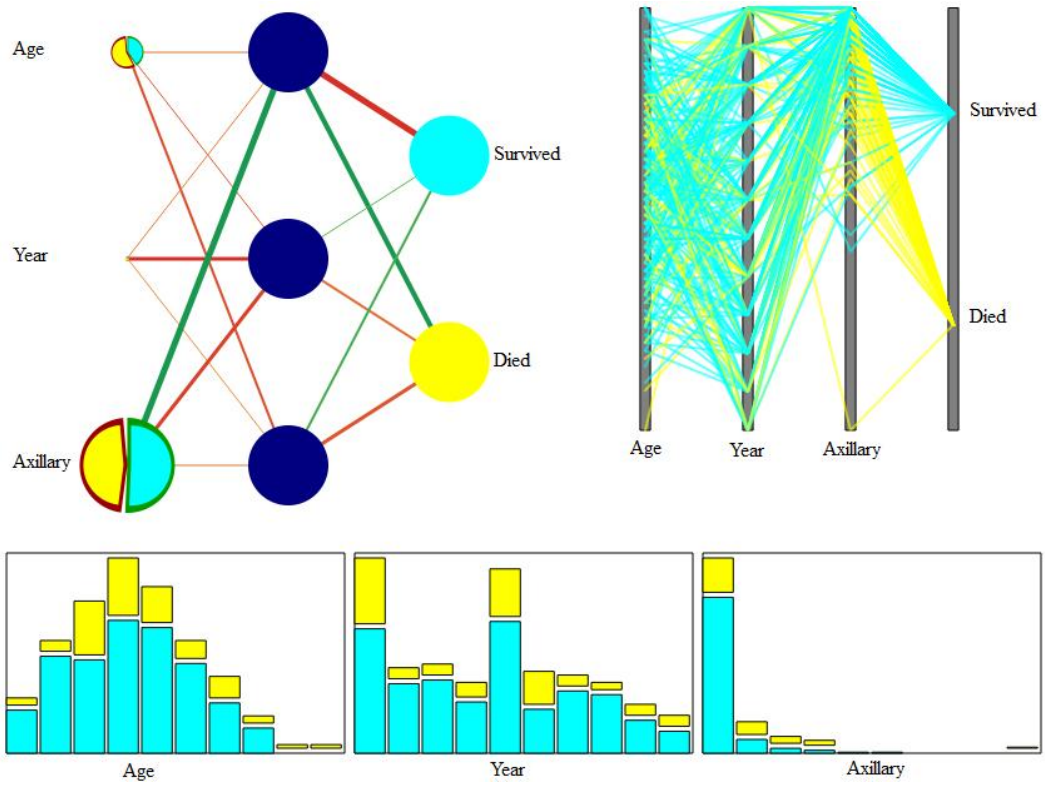

Figure 2. Visualization of input contribution. (Top left) neural network visualization of input and weight contributions, (top right) parallel coordinates plot shows the distribution and relation between inputs and outputs, (bottom) data histogram plot shows data distribution over output classes.

visualization on the *Haberman's Survival* dataset (Bache and Lichman, 2013) which consists of three input variables (age of patient at time of operation, patient's year of operation, and number of positive axillary nodes detected) and two output classes (the patient survived five years or longer and the patient died within 5 years). As shown in Figure 2, the total contribution of a unit towards the class output is represented by the size of that input unit. Within a unit, sectors represent the effect of that input unit with respect to each output class. The sector size signifies the magnitude of the contribution while color indicates to which particular output. As described earlier, input contribution can be positive or negative. Therefore, sectors are surrounded by bands of red color for positive contribution and green color for negative contribution.

Figure 2 clearly shows that *Axillary* has a strong effect on the class output, while *Age* and *Year* have moderate and low effect, respectively. To investigate our results we plot the parallel coordinates Figure 2 (top right) and data histogram Figure 2 (bottom) to study the structure and distribution of the dataset. The plots show that for the less significant inputs (*Age* and *Year*) both classes (*Survived* and *Died*) occur over most of the data range while for *Axillary* the classes do not span the entire range of data; for instance, only *Died* occurs in the upper range of data which makes *Axillary* a more decisive input variable. Besides the overall contribution of inputs, Figure 2 suggests that *Axillary* negatively contributes to output class *Survived* and positively contributes to *Died*.

Weight visualization

The knowledge gained by the neural network is stored, in its entirety, in the network weights. In our visualization, we represent weights as varying-width color coded edges. The width indicates the magnitude of contribution and the color (red for positive and green for negative) indicates the sign of contribution. Figure 2 shows the visualization of connection weights. Most significant weights, for instance the weight between *Axillary* and hidden 1 and weights between hidden 1 and both output classes (*Survived* and *Died*) are readily conceivable which supports our previously mentioned findings.

Sensitivity visualization

Our approach for visualizing sensitivity is similar to our visualization of input contribution previously discussed, where unit size indicates the significance of input and

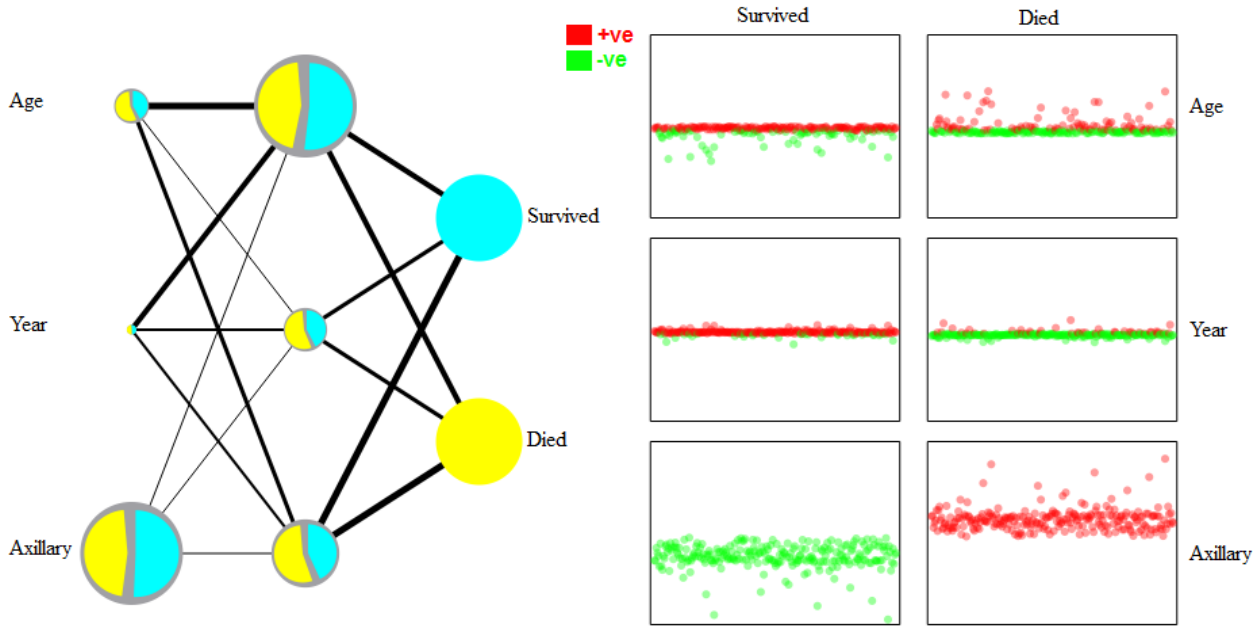

Figure 3. Visualization of sensitivity analysis. (Left) neural network visualization of sensitivity analysis, (right) plot of changes of output for every pattern in the dataset.

hidden units, and edge width indicates the network weights. Unit sectors determine the significance with respect to each output class. As described in Equation 5, sensitivity is defined by the maximum change of input with respect to output class; therefore it does not carry a positive or negative sign. Figure 3 (left) shows an example of our sensitivity visualization. Sectors are slightly spread out and laid over a gray background color to enhance the visual comprehension. In Figure 3 (right), we plot the sensitivity of output classes (*Survived* and *Died*) due to changes in input variables (*Age*, *Year*, and *Axillary*) for every pattern in the dataset. This plot further justifies our findings in Figure 3 (left). It is clearly obvious that *Axillary* is the most influential variable and as suggested by Figure 3 (right) it positively changes with respect to *Died* class and negatively with respect to *Survived* class.

INPUT PRUNING AND ERROR ANALYSIS

When receiving training on a neural network, one should use the smallest system that will fit the data (Reed, 1993). Unfortunately, this is rarely the case because datasets usually contain a lot of noise data that does not contribute much and even slows the learning. In input pruning, we leave out less important features and evaluate the error; if the network performance deteriorates beyond an acceptable rate we plug the features back.

Figure 4 shows an example of our visualization on the *Car Evaluation* dataset (Bache and Lichman, 2013). It contains 6 input variables (*buying*, *maintenance*, *doors*, *persons*, *lug boot* and *safety*) and 4 output classes (*unacceptable*, *acceptable*, *good*, *very good*) and 1728 instances. Figure 4(a) and (b) show visualizations of input contributions and sensitivity analysis, respectively. The figures show that *Safety* contributes the most to the class output and that both *Safety* and *Persons* are the most influential input variables. The figures suggest that the remaining input variables are less important and can be excluded to reduce the complexity of domain.

A common way to carry out input pruning while maintaining acceptable results consists of comparing errors made by the network from the original patterns with the errors made with excluding the input of interest. In Figure 5, we plot error rates resultant from pruning less important inputs. Figure 5 (row 1, left) shows the error rate when including all 6 inputs. Pruning the less important inputs *doors*, *lug boot*, and *maintenance* improves the error rates as shown in Figure 5 (row 1, right), (row 2, left), and (row 2, right), respectively. As expected, the error increases when more important inputs are pruned as shown when inputs *buying* Figure 5 (row 3, left) and input *persons* Figure 5 (row 3, right) are left out. The figure also shows the change of error for each output class due to pruned inputs. The results shown in the figure supports our findings.

Conclusion

We seek to promote the understanding of neural network internal structures by presenting a visualization approach

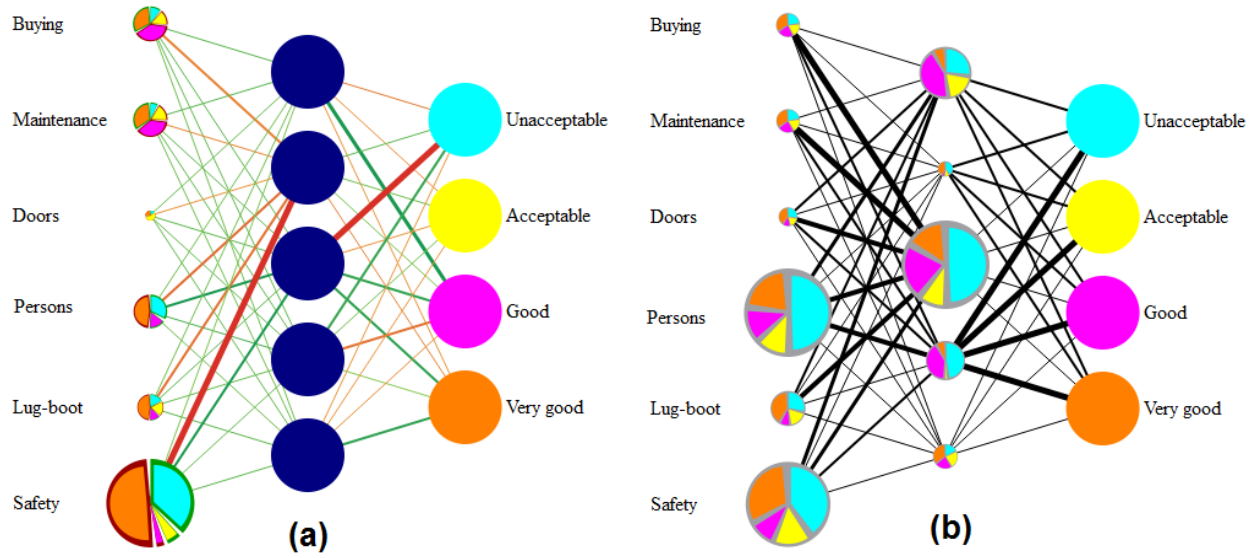

Figure 4. Visualization of car evaluating dataset. (a) input contribution visualization (b) sensitivity analysis visualization.

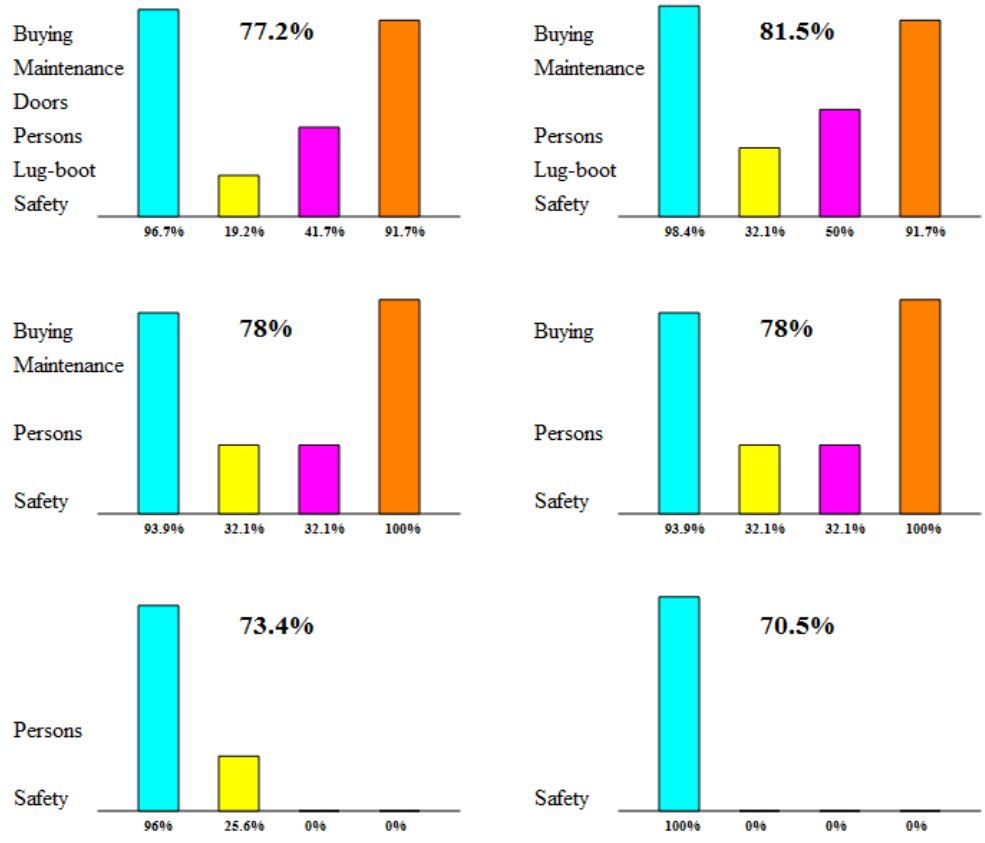

Figure 5. Visualization of error rates after pruning less significant input variables.

that is capable of enhancing the perception of input contributions and reducing the complexity of domain problems. Our approach guides the pruning of less important features found via visual representations of input contributions and sensitivity analysis. We show that our approach can maintain a high rate of performance of

a neural network while excluding noise data and less influential features.

Conflict of Interests

The author(s) have not declared any conflict of interests.

REFERENCES

Abraham A (2004). Meta learning evolutionary artificial neural networks. Neurocomput. 56:1-38. http://dx.doi.org/10.1016/S0925-2312(03)00369-2

Bache K, Lichman M (2013). UCI Machine Learning Repository [http://archive.ics.uci.edu/ml/]. Irvine, CA: University of California, School of Information and Computer Science.

Engelbrecht A, Cloete I (1998). Feature extraction from feedforward neural networks using sensitivity analysis.In Proceedings of the International Conference on Systems, Signals, Control, Computers, pp. 221-225.

Fischer I, Zell A (2000).Visualization of neural networks using java applets. In Proceedings of the 11th Annual Conference of the EAEEIE. pp. 71–76.

Garson GD (1991). Interpreting neural-network connection weights. AI Expert 6(4):46-51.

Gevrey M, Dimopoulos I, Lek S (2003). Review and comparison of methodsto study the contribution of variables in artificial neural network models. Ecol. Model. 160(3):249-264. http://dx.doi.org/10.1016/S0304-3800(02)00257-0

Goh ATC (1995). Back-propagation neural networks for modeling complex systems.AI Eng. 9(3):143-151.

Haykin S (1999). Neural Networks: A Comprehensive Foundation. Princeton Hall, 2nd Edition.

Milne L (1995). Feature selection using neural networks with contribution measures. AI-Conference pp. 571-571.

Montao JJ, Palmer A (2003). Numeric sensitivity analysis applied to feedforward neural networks. Neural Comput. Appl. 12(2):119-125. http://dx.doi.org/10.1007/s00521-003-0377-9

Olden JD, Jackson DA (2002). Illuminating the black box: A randomization approach for understanding variable contributions in artificial neural networks. Ecol. Model. 154(1):135-150. http://dx.doi.org/10.1016/S0304-3800(02)00064-9

Paliwal M, Kumar UA (2011). Assessing the contribution of variables in feed forward neural network. Appl. Soft Comput. 11(4):3690-3696. http://dx.doi.org/10.1016/j.asoc.2011.01.040

Reed R (1993). Pruning algorithms - A survey. IEEE Trans. Neural Netw. 4(5):740-747. http://dx.doi.org/10.1109/72.248452

Sjöberg J, Zhang Q, Ljung L, Benveniste A, Delyon B, Glorennec PY, Hjalmarsson H, Juditsky A (1995). Nonlinear black-box modeling in system identification: A unified overview. Automatica 31(12):1691-1724. http://dx.doi.org/10.1016/0005-1098(95)00120-8

Steeler MJ, Ward MO, Alvarez SA (2001). Nvis: An interactive visualization tool for neural networks. In Proceedings of SPIE Symposium on Visual DataExploration and Analysis. pp. 234–241.

Tzeng FY, Ma KL (2005). Opening the black box - Data driven visualization of neural network. IEEE Visualization. p. 49.

Viste M, Skartveit HL (2004). Visualization of complex systems - The two shower mode. Psychnol. J. 2(2):229-241.

academicJournals

Related Journals Published by Academic Journals

- International NGO Journal
- International Journal of Peace and Development Studies